Acta Biomaterialia 137 (2022) 218–237

Contents lists available at ScienceDirect

Acta Biomaterialia

journal homepage: www.elsevier.com/locate/actbio

Full length article

Arabic gum plus colistin coated moxifloxacin-loaded nanoparticles for the treatment of bone infection caused by *Escherichia coli*

J.J. Aguilera-Correa[a,b,1], M. Gisbert-Garzarán[a,c,1], A. Mediero[d], R.A. Carias-Cálix[e], C. Jiménez-Jiménez[a,c], J. Esteban[b,f,*], M. Vallet-Regí[a,c,*]

[a] Departamento de Química en Ciencias Farmacéuticas, Universidad Complutense de Madrid, Instituto de Investigación Sanitaria Hospital 12 de Octubre i+12, Plaza Ramón y Cajal s/n, Madrid 28040, Spain
[b] Networking Research Centre on Infectious Diseases (CIBER-ID), 28029 Madrid, Spain
[c] Networking Research Centre, Bioengineering, Biomaterials and Nanomedicine (CIBER-BBN), Madrid 28029, Spain
[d] Bone and Joint Unit, IIS- Fundación Jimenez Diaz, UAM, Avenida Reyes Católicos, 2, Madrid 28037, Spain
[e] Pathology Department, Fundacion Jimenez Diaz University Hospital, UAM, Madrid, Spain
[f] Clinical Microbiology Department, IIS-Fundación Jiménez Diaz, UAM, Avenida Reyes Católicos, 2, Madrid 28037, Spain

ARTICLE INFO

Article history:
Received 3 August 2021
Revised 20 September 2021
Accepted 7 October 2021
Available online 13 October 2021

Keywords:
Osteomyelitis
Escherichia coli
Biofilm
Nanoparticles
Arabic gum
Colistin
Moxifloxacin

ABSTRACT

Osteomyelitis is an inflammatory process of bone and bone marrow that may even lead to patient death. Even though this disease is mainly caused by Gram-positive organisms, the proportion of bone infections caused by Gram-negative bacteria, such as *Escherichia coli*, has significantly increased in recent years. In this work, mesoporous silica nanoparticles have been employed as platform to engineer a nanomedicine able to eradicate *E. coli*- related bone infections. For that purpose, the nanoparticles have been loaded with moxifloxacin and further functionalized with Arabic gum and colistin (AG+CO-coated MX-loaded MSNs). The nanosystem demonstrated high affinity toward *E. coli* biofilm matrix, thanks to AG coating, and marked antibacterial effect because of the bactericidal effect of moxifloxacin and the disaggregating effect of colistin. AG+CO-coated MX-loaded MSNs were able to eradicate the infection developed on a trabecular bone *in vitro* and showed pronounced antibacterial efficacy *in vivo* against an osteomyelitis provoked by *E. coli*. Furthermore, AG+CO-coated MX-loaded MSNs were shown to be essentially non-cytotoxic with only slight effect on cell proliferation and mild hepatotoxicity, which might be attributed to the nature of both antibiotics. In view of these results, these nanoparticles may be considered as a promising treatment for bone infections caused by enterobacteria, such as *E. coli*, and introduce a general strategy against bone infections based on the implementation of antibiotics with different but complementary activity into a single nanocarrier.

Statement of significance

In this work, we propose a methodology to address *E.coli* bone infections by using moxifloxacin-loaded mesoporous silica nanoparticles coated with Arabic gum containing colistin (AG+CO-coated MX-loaded MSNs). The *in vitro* evaluation of this nanosystem demonstrated high affinity toward *E. coli* biofilm matrix thanks to the Arabic gum coating, a disaggregating and antibacterial effect of colistin, and a remarkable antibiofilm action because of the bactericidal ability of moxifloxacin and colistin. This anti-*E. coli* capacity

Abbreviations: AG, arabic gum; AG+CO, arabic gum containing colistin; APTES, 3-(aminopropyl)triethoxysilane; BHI, brain-heart infusion; CAMHB, cation adjusted Müller-Hinton broth; CFU, colony-forming unit; CO-FITC, colistin labeled with fluorescein isothiocyanate; CO, colistin; CTAB, cetyltrimethylammonium bromide; Cyp3A, cytochrome P450 3A4; DLS, dynamic Light Scattering; DMSO, dimethyl sulfoxide; FTIR, Fourier transformed Infrared; GFP, green fluorescent protein; HBSS, Hanks' balanced saline solution; Hs, hepatocytes; IL-6, interleukine 6; KCs, Kupffer cells; MBC, minimum bactericidal concentration; MBEC, minimum biofilm eradication concentration; MBIC, minimum biofilm inhibitory concentration; MIC, minimum inhibitory concentration; MSNs, mesoporous silica nanoparticles; MX, RhB moxifloxacin; NPCs, non-parenchymal cells; PBS, phosphate buffer saline; PI, propidium iodide; RANKL, receptor activator for nuclear factor κ B Ligand; RhB, Rhodamine B isothiocyanate; SEM, scanning electron microscopy; TEOS, tetraethyl orthosilicate; TGA, thermogravimetric Analysis; TNF-α, tumour necrosis factor α; TVX, trovafloxacin.

* Corresponding authors at: Departamento de Química en Ciencias Farmacéuticas, Universidad Complutense de Madrid, Plaza Ramón y Cajal s/n, Madrid 28040, Spain.
E-mail addresses: john_j2a@hotmail.com (J.J. Aguilera-Correa), migisber@ucm.es (M. Gisbert-Garzarán), aranzazu.mediero@quironsalud.es (A. Mediero), rafael.carias@quironsalud.es (R.A. Carias-Cálix), carlaj05@ucm.es (C. Jiménez-Jiménez), jestebanmoreno@gmail.com (J. Esteban), vallet@ucm.es (M. Vallet-Regí).
[1] These authors contributed equally to this work.

https://doi.org/10.1016/j.actbio.2021.10.014

of AG+CO-coated MX-loaded MSNs was brought out in an *in vivo* rabbit model of osteomyelitis where the nanosystem was able to eradicate more than 90% of the bacterial load within the infected bone.

1. Introduction

Osteomyelitis is an inflammatory process of bone and bone marrow caused by at least one microorganism, which causes local bone destruction, necrosis, and apposition of new bone and can compromise bone or joint infection [1]. Despite its incidence is almost 22 cases per 100,000 person-years [2], the implications of this disease are beyond these numbers, including mortality [3].

Although osteomyelitis can be virtually caused by any microorganism, bone infections are mainly caused by Gram-positive bacteria, such as *Staphylococcus aureus*, which is responsible for up to 90% of the cases of pyogenic osteomyelitis [1]. However, the proportion of bone infections caused by Gram-negative bacteria has significantly increased over the last few years [4,5]. Among them, enterobacteria, like *Escherichia coli*, have attracted much attention owing to their ability to reach antibiotic multi-resistance [6,7]. Besides, the bacterial pathogeny of this infection involves the biofilm development, which is a growth form increases the resistance to multiple adverse situations, including phagocytosis by phagocytic cells from immune systems, as well as antibiotics [8]. For this reason, the most frequent treatments for osteomyelitis include intravenous antibiotic administration together with surgical removal of portions of infected or dead bone [9,10].

In the last few decades, the application of nanotechnology to medicine, so-called nanomedicine, has attracted much attention and it is expected to revolutionize the biotechnological and pharmaceutical industries shortly. In this regard, nanoparticles acting as drug delivery vehicles account for 75% of the market share of approved nanomedicines [11]. Among the different types of nanocarriers, mesoporous silica nanoparticles (MSNs) are considered as promising candidates for drug delivery owing to features, such as large surface areas (*ca.* 1,000 m^2/g) and pore volumes (*ca.* 1 cm^3/g), tunable pore size and morphologies, ease of surface modification, and biocompatibility [12–15]. As a result, MSNs have been widely applied to treat several diseases, including complex bone diseases, such as osteoporosis, bone cancer and bone infection [16]. Regarding the latter, the suitability of loading MSNs with low-molecular-weight antibiotics for eliminating *E. coli* bone infections has been reported [17–19]. Aside from treating bone infections, endowing the nanoparticles with ability to recognize infection is of major importance. In this regard, some authors have reported the use of antibodies, aptamers, dendrimers, or proteins, among others, to target bone infection [20].

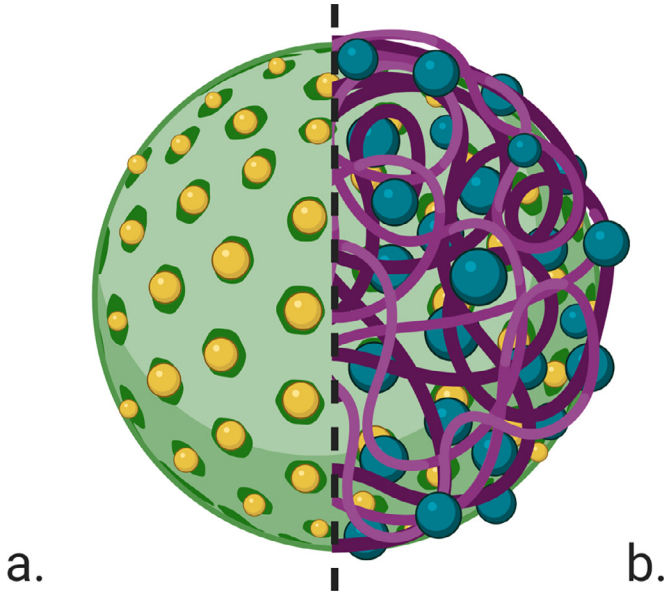

Scheme 1. Mesoporous silica nanoparticles (green) loaded with moxifloxacin (yellow) (a) and coated with Arabic gum (purple) plus colistin (blue).

In this work, we have employed MSNs to engineer a drug delivery nanovehicle for the potential treatment of bone infections caused by *E. coli* (Scheme 1). Because of the potential translation of this nanomaterial, two clinically relevant antibiotics, moxifloxacin (MX) and colistin (CO), were selected as payloads. MX is a fourth-generation fluoroquinolone antibacterial agent with a broad spectrum of activity, encompassing Gram-negative and Gram-positive bacteria [21], that has been used in monotherapy in bone-related infection [22–24]. CO is a polymyxin agent (polymyxin E) that has proven to be effective against Gram-negative infections [25], and was selected because of its anti-*E. coli* ability vouched by previous *in vitro* and *in vivo* studies of prosthetic joint infection [26]. Given the pivotal role of biofilm formation during this type of infection, we aimed to endow MSNs with selectivity for the *E. coli* biofilm model to enhance the efficacy of the treatment. For that purpose, the surface of nanoparticles was modified with Arabic gum (AG), a branched-chain, complex polysaccharide composed of 1,3-linked beta-D-galactopyranosyl monomers connected to the main chain through 1,6-linkages [27], whose degradation by secreted bacterial enzymes was observed to improve the retention of MSNs on the biofilm. Furthermore, it was observed that the use of the AG coating improved the adsorption of CO on the surface of MSNs. Finally, the bactericidal effect of this biocompatible nanocarrier was extensively analysed *in vitro* and *in vivo*, showing promising results. To the best of our knowledge, this is the first time that MSNs are engineered to carry low molecular weight and a high molecular weight antibiotic at the same time, instead of just one antibiotic, while achieving significant targeting capacity for *E. coli* biofilm and substantial efficacy *in vivo*.

2. Materials and methods

2.1. Synthesis of MCM-41 mesoporous silica nanoparticles

The following compounds were purchased from Sigma-Aldrich (USA): Tetraethyl orthosilicate (TEOS); Ammonium nitrate; Cetyltrimethylammonium bromide (CTAB); Rhodamine B isothiocyanate (RhB); 3-(Aminopropyl) triethoxysilane (APTES).

Mesoporous silica nanoparticles were synthesized through a modification of the Stöber method [28]. For that purpose, H_2O (480 mL), NaOH (2 M, 3.5 mL) and CTAB (2.74 mmol, 1 g), were mixed in a 1-L flask and heated to 80 °C. Then, TEOS (22.39 mmol, 5 mL) was added dropwise (0.33 mL/min) over 15 min and the whole mixture was then stirred at 80 °C for 2 h. After that, the nanoparticles were collected by centrifugation and washed twice with water and once with ethanol. The organic template was removed by ionic exchange, using a solution of NH_4NO_3 (10 mg/mL)

in ethanol (95%). For that purpose, nanoparticles were dispersed in 350 mL of such solution, refluxed for 3 h and subsequently centrifuged and washed with water and ethanol. The whole process was repeated two times, and the final surfactant-free nanoparticles were stored in absolute ethanol.

The biological experiments were performed using Rhodamine B-labeled MSNs. For this end, RhB (0.002 mmol, 1.07 mg) was reacted with APTES (0.009 mmol, 2.2 µL) in 40 µL of ethanol for 2 h. Then, this mixture was gently mixed with TEOS (22.39 mmol, 5 mL) and the synthesis of MSNs was carried out as described above.

The nanoparticles were characterized in terms of Fourier Transformed Infrared (FTIR) spectroscopy, Thermogravimetric Analysis (TGA), Dynamic Light Scattering (DLS), Zeta potential, and N_2 adsorption analysis. FTIR spectra were collected in a Nicolet Nexus (Thermo Fisher Scientific) equipped with a Goldengate attenuated total reflectance device, averaging 64 scans in the range 4,000–400 cm^{-1} (resolution 1 cm^{-1}). TGA measurements were carried out in a Perkin Elmer Pyris Diamond TG/DTA analyser, applying 5 °C/min heating ramps from rt to 600 °C. DLS and Zeta potential measurements were performed in a Zetasizer Nano ZS (Malvern Instruments) equipped with a 633 nm laser. Samples were dispersed in distilled water with sonication and placed in a DTS1070 disposable folded capillary cell (Malvern instruments) for data acquisition. N_2 adsorption analysis (adsorption and desorption isotherms) were obtained in a Micromeritics ASAP 2020. Samples were degassed under vacuum for 24 h and analyzed at 77 K. Pore size was estimated from the maximum of the pore size distribution plot.

2.2. Arabic gum coating of nanoparticles and antibiotic release from coated nanoparticles

Arabic gum coating was performed by adapting a methodology previously described [29]. The use of Arabic gum is based on the enterobacterial ability to degrade and use it as carbon source [30,31]. MSNs were initially functionalized with AG before the antibiotics incorporation to find out the conditions that provided significant AG deposition onto the surface. Briefly, Arabic gum (10%, w/v) was prepared by dissolving 4 g of Arabic gum from acacia tree powder (Sigma Aldrich, USA) in 20 mL distilled water. The solution was stirred with low heat (40–45 °C) for 60 min using a hot plate magnetic stirrer and was left to cool down to room temperature. Then, 1 mL of Arabic gum 10% was deposited in a 4 mL glass recipient under vigorous agitation at room temperature and mixed with 1 mL of water with 12 mg/mL of MSNs for 10 min. Then, the nanoparticles were centrifuged and washed twice with distilled water, leading to AG-coated MSNs.

For the synthesis of Arabic gum plus colistin-coated MSNs, 50 mg of colistin sodium methanesulfonate (Sigma Aldrich, USA) were mixed with 1 mL of Arabic gum 10% and the coating was carried out as described above to yield AG+CO-coated MSNs.

The coated nanoparticles were characterized in terms of Fourier Transformed Infrared (FTIR) spectroscopy, Thermogravimetric Analysis (TGA), Transmission Electron Microscopy (TEM), Dynamic Light Scattering (DLS) and Zeta potential. TEM images were taken on a JEOL JEM 1400. Samples were dispersed in distilled water under sonication and then few drops were deposited onto carbon-coated copper grids.

2.3. Antibiotic loading into the nanoparticle and antibiotic release

One millilitre of a 5 mg/mL solution of moxifloxacin (Sigma Aldrich, USA) (MX) in HEPES buffer [32] (Lonza, Switzerland) was added to 12 mg of MSNs. These MSNs were loaded at 500 rpm and 5 °C for 24 h [33]. After loading, MSNs were washed two times with HEPES buffer (MX-loaded MSNs).

To determine the moxifloxacin release from loaded MSNs, 12 mg of MSNs were suspended in 1 mL of phosphate buffer saline (PBS) (pH = 7.4) (Lonza, Switzerland). This suspension was placed with another millilitre of PBS into the lower chamber from a Transwell® 6-well plate (Corning, USA). Then, the upper chamber of the Transwell® 6-well plate was placed and 1 mL of PBS was added. This buffer was selected because is one of the most used buffer for antibiotic release [34–38]. The final concentration of nanoparticles was 4 mg/mL per well ($n = 4$). The plate was incubated at 37 °C and 5% CO_2. Periodically, 300 µL of each upper chamber from well were sampled and replaced by 300 µL of new PBS. These 300 µL were used to determine moxifloxacin concentration by measuring the fluorescence using an excitation wavelength of 294 nm and an emission wavelength of 503 nm [39], and a calibration curve made with a concentration range from 125 to 0.122 µg/mL. This experiment was performed four times.

To determine the colistin release from Arabic gum plus colistin coated MSNs, 12 mg of MSNs were coated with 50 mg of colistin in presence or absence of 1 mL of Arabic gum 20%. Colistin previously labeled with fluorescein isothiocianate (CO-FITC) to monitor the release. For that reason, 50 mg of colistin and 0.1 mg of FITC were dissolved in DMSO and stirred overnight at RT. The mixture was then precipitated in cold ether/acetone (90:10), centrifuged and washed with ethanol until no FITC was observed in the supernatant. CO-FITC MSNs were suspended in 1 mL of phosphate buffer saline (PBS) (Lonza, Switzerland) to evaluate the release kinetics. This millilitre was placed with another millilitre of PBS into the lower chamber from a Transwell® 6-well plate (Corning, USA). Then, the upper chamber of the Transwell® 6-well plate was placed and 1 mL of PBS was added. The final concentration of nanoparticles was 4 mg/mL per well ($n = 3$). The plate was incubated at 37 °C and 5% CO_2. Regularly, 300 µL of each upper chamber from well were sampled and replaced by 300 µL of new PBS. These 300 µL were used to determine colistin-FITC concentration by measuring the fluorescence using an excitation wavelength of 490 nm and an emission wavelength of 525 nm, and a calibration curve made with a concentration range from 500 to 0.244 µg/mL.

2.4. Microbiological studies

E. coli ATCC 25922-GFP strain was used in all microbiological studies. This strain can produce a green fluorescent protein (GFP). The strain was kept frozen at –80 °C until experiments were performed. According to the recommendations of the commercial house, this strain was grown in tryptic soy broth (BioMérieux, France) supplemented with 100 µg/mL of ampicillin (Merck, USA) at 37 °C in 5% CO_2. The purity of its axenic culture was corroborated every day by inoculating each broth on a blood tryptic-soy agar (BioMérieux, France).

2.4.1. Bacteria-nanoparticle interaction

The *E. coli*-nanoparticle interaction was evaluated by using four different experiments, (1) use of Arabic gum coating as a carbon source by *E. coli*, (2) *E. coli* biofilm-nanoparticles interaction, (3) bactericidal ability of Arabic gum plus colistin coating against *E. coli* and, (4) *E. coli* effect on the release of drugs loaded in the nanoparticles.

To evaluate the use of Arabic gum coating as a carbon source by *E. coli*, 500 µL of PBS with 10 mg/mL (1% p/v) of each type of nanoparticle (MSNs and AG-coated MSNs) were deposited in a well from a 24-well plate. Then, 10 µL of a bacterial suspension with 3.18×10^6 CFU/mL were added. PBS supplemented with 1% of Arabic gum was used as positive control. Then, the plate was incubated statically at 37 °C and 5% CO_2 for 24 h. After incubation, 300 µL of each well were placed in a 96-well flat-bottom plate

(Thermo Fisher Scientific, USA) and their fluorescence was measured using an excitation wavelength of 488 nm and an emission wavelength of 510 nm. This experiment was performed by duplicate and four times ($n = 8$ per condition).

To describe the *E. coli* effect on the release of drugs loaded in AG-coated MSNs, 12 mg of MSNs were loaded with 500 µL of propidium iodide (PI) in water (500 µg/mL) (Sigma Aldrich, USA) at 750 rpm and 5 °C for 24 h. After loading, these nanoparticles were rinsed one time with 1 mL of distilled water. After this, 12 mg of each PI-loaded MSNs were suspended in 1 mL of brain-heart infusion (BHI) (BD, USA) to determine the PI release from AG-coated PI-loaded and noncoated PI-loaded MSNs. This suspension was mixed 1:1 with another suspension (10^8 CFU/mL of bacteria in BHI) into the lower chamber from a Transwell® 6-well plate. Then, the upper chamber of the Transwell® 6-well plate was inserted and 1 mL of BHI was added. The final concentration of nanoparticles was 4 mg/mL per well. The plate was incubated at 37 °C and 5% CO_2. Periodically, 300 µL of each upper chamber from well were sampled and replaced by 300 µL of sterile BHI. These 300 µL were used to determine the PI concentration by measuring the fluorescence using an excitation wavelength of 493 nm and an emission wavelength of 636 nm, and a calibration curve made with a concentration range from 250 to 0.122 µg/mL. The bacterial concentration was estimated by using a well from a 6-well plate with the same bacterial concentration but without MSNs. This experiment was performed by triplicate.

To study *E. coli* biofilm-nanoparticles interaction, 100 µL of saline 0.9% NaCl (B. Braun, Germany) with 3.23×10^8 CFU/mL were placed in each well of a 96-well flat-bottom plate and incubated statically at 37 °C and 5% CO_2 for 1.5 h. The supernatant was then removed, and each well was rinsed two times with 150 µL of saline. Then, 200 µL of wound-like medium were added to each well, and the plate was incubated statically at 37 °C and 5% CO_2 for 48 h. Wound-like medium is composed by 5 mL of Bolton broth (Sigma Aldrich, USA), 4.5 mL of bovine adult serum (Sigma Aldrich, USA), and 0.5 mL of laked horse blood (Oxoid, USA) [40,41]. The use of wound-like medium had no other purpose but mimicking *in vitro* the nutritional conditions that a bacterium causing bone infection could find *in vivo*. After incubation, the supernatant was removed, and each well was rinsed two times with 200 µL of saline. Then, 150 µL of saline with 2 mg/mL of each type of MSN (MSN, AG-coated MSN, and AG+CO-coated MSNs) were added to the corresponding wells and incubated at 100 rpm, 37 °C, and 5% CO_2 for 30 min and 3 h. After that, each well was rinsed again with 200 µL of saline and stained with 1% of safranin, according to a previously reported methodology [42]. The experiment was performed by triplicate ($n = 24$ per condition).

To demonstrate the bactericidal ability of Arabic gum plus colistin coating against *E. coli*, 500 µL of saline with 1×10^8 CFU/mL plus 500 µL of saline with 4 mg/mL of each type of nanoparticle (MSNs, AG-coated MSNs, and AG+CO-coated MSNs) were placed in a 2 mL tube (final concentration of 2 mg/mL). This concentration of bacteria was chosen to bring to light the antibacterial effect of MSNs without needing the bacterial growth. Each tube was agitated at 1.400 rpm and 37 °C for 30 min. After this, 150 µL of each tube were mixed with 150 µL of tryptic-soy broth supplemented with 20% alamarBlue (BIO-RAD, USA) [43] in a well from a 96-well flat-bottom plate, and were incubated at 100 rpm and 37 °C for 2 h. The fluorescence from each well was then measured using an excitation wavelength of 560 nm and an emission wavelength of 590 nm. This experiment was performed four times ($n = 4$ per condition). To support visually the numerical results, the previous experiment was analysed using transmission electron microscopy (TEM). The protocol for TEM has been described previously [44]. Semithin sections (0.6 µm) for light microscopy and thin sections (60 nm) for TEM of resin-included bacteria were cut using a Leica Ultracut ultramicrotome UC7 (Leica). Sections were collected on 200 mesh nickel grids and examined using a Jeol JEM 1400 transmission electron microscope (Jeol Ltd, Tokyo, Japan).

2.4.2. Minimal inhibitory concentration and minimal bactericidal concentration

Minimum inhibitory concentrations (MIC) were determined using the previously described broth microdilution method [45] with one modification. The MIC is the minimum concentration required to inhibit the bacterial visible growth. The main modification consisted of supplementing all the broth used with 100 µg/mL of ampicillin. In brief, a series of nanoparticle concentrations starting from 2,000 to 1.953 µg/mL with a two-fold dilution were added to cation adjusted Müller-Hinton broth (Sigma Aldrich, USA) (CAMHB) to a final volume of 100 µL per well. One hundred microlitres of bacterial suspension in CAMHB containing approximately 1.6×10^6 colony-forming units per millilitre (CFU/mL) was added to a Costar 96-well round-bottom polypropylene plate (Corning Inc., USA) followed by static incubation at 37 °C and 5% CO_2 for at least 20 h. After incubation, MIC was determined measuring fluorescence using an excitation wavelength of 488 nm and an emission wavelength of 510 nm. Minimum bactericidal concentration (MBC) were determined using the flash microbiocide method previously described [46] . The MBC is defined as the minimum concentration required to kill a certain bacterial concentration. Briefly, 10 µL of each well were mixed after 24 h incubation with 190 µL of tryptic soy broth in a new 96-well plate, which was further incubated statically at 37 °C and 5% CO_2 for 24 h. After incubation, MBC was determined by measuring the fluorescence, using an excitation wavelength of 488 nm and an emission wavelength of 510 nm. The experiments were performed by triplicate.

2.4.3. Minimal biofilm inhibitory concentration and minimal biofilm eradication concentration

Minimal biofilm inhibitory concentrations (MBIC) and minimal biofilm eradication concentrations were determined using the methodology previously described [47]. The MBIC is the minimum concentration required to inhibit the visible growth of a bacterial biofilm. For MBIC, biofilm formation on pegs from the Calgary device was induced by inoculating 200 µL of tryptic-soy broth containing 10^6 CFU/mL of bacteria per well in a 96-well flat-bottom plate (Thermo Fisher Scientific, Massachusetts, United States). The lid (Thermo Fisher Scientific) of the Calgary device was then placed and the plate was incubated in turmoil at 37 °C and 5% CO_2 for 24 h. After incubation, the pegs from the lid were rinsed two times in wells containing 200 µL of saline. Afterwards, the lid was placed in a plate with different MSN concentrations starting from 2,000 to 1.953 µg/mL with a two-fold dilution were added to CAMHB to a final volume of 200 µL per well and was incubated by static incubation at 37 °C and 5% CO_2 for at least 20 h. After incubation, MBIC was determined by measuring the fluorescence, using an excitation wavelength of 488 nm and an emission wavelength of 510 nm. The MBEC is the minimum concentration required to kill a bacterial biofilm. For MBEC, the lid from the MBIC was rinsed two times in a plate with wells containing 200 µL of saline 0.9% NaCl, placed in a plate with 200 µL of tryptic-soy broth, and incubated statically at 37 °C and 5% CO_2 for 24 h. After incubation, MBEC was determined by measuring the fluorescence, using an excitation wavelength of 488 nm and an emission wavelength of 510 nm. The experiments were performed by triplicate.

2.4.4. Anti-biofilm efficacy of AG+CO-coated MX-loaded MSNs

A four-mL flat-bottom sterile tube with 25 mg of bovine trabecular bone (Bio-Oss Spongiosa from 0.25 to 1 mm; Inibsa, Spain) was rinsed with 1 mL of saline. Then, 500 µL of saline with 3.15×10^8 CFU/mL were added to each tube and were incubated

statically at 37 °C and 5% CO_2 for 1.5 h. The supernatant was then removed, and each tube was rinsed two times with 1 mL of saline. Afterward, 1 mL of wound-like medium were placed into each tube, which were further incubated statically at 37 °C and 5% CO_2 for 48 h. The wound-like medium is a biofilm model that resembles the type of biofilm that is usually found in clinical practice [48]. The rationale for using this medium relies on its composition. Among others, this wound-like medium contains erythrocytes and serum, which are components that the nanoparticles would have to deal with in an infection in a human body. Hence, the purpose of using bovine trabecular bone and wound-like medium was to mimic *in vitro* in a very realistic way the conditions where a bacterium causing osteomyelitis would grow *in vivo*. After biofilm formation, each tube was rinsed two times with 1 mL saline and treated in presence or absence of 1 mL of two effective concentrations of nanoparticles, which were further incubated statically at 37 °C and 5% CO_2 for 24 h. Such concentrations, 31.25 and 62.5 µg/mL, were estimated according to the MBEC obtained, and considering previous studies that stablish 4 × MIC as a good therapeutic approach [32,49]. After incubation, each tube was rinsed two times with 1 mL of saline and all trabecular bone from each tube were transferred to a 5 mL round-bottom tube containing 1 mL of saline. All tubes were sonicated at room temperature for 5 min [50]. Then, the number of bacteria was determined as CFU per gram of bone by using the drop plate method [51] in MacConkey agar plates (BioMérieux, France). The plates were incubated at 37 °C and 5% CO_2 at least 24 h. The experiment was performed five times.

To support visually the numerical results, the previous experiment was analysed using laser confocal microscopy and scanning electron microscopy (SEM). For laser confocal microscopy, the experiment was performed in a 4 × 2 glass-bottom plate (ibidi, Germany) where the tubes were replaced by wells, and all the abovementioned volumes were replaced by 300 µL of each medium. After 24 h, each well was directly analysed in a Leica DM IRB confocal laser-scanning microscope (Leica, Germany) without removing the supernatant. For SEM study, the same samples were fixed with 2.5% glutaraldehyde in 0.1 M sodium cacodylate buffer at pH7 at 4 °C for 90 min. Samples were then dehydrated with increasing concentrations of ethanol (30, 50, 70, 90, and 100%) at 22 °C for 10 min. Micrographs were obtained using a field emission gun JEOL JSM6400 scanning electron microscope (Jeol Ltd, Tokyo, Japan).

2.5. Cell studies

MC3T3-E1 cells were inoculated in a concentration of 10,000 cells/cm^2 on 96-well plates with α-minimum essential medium with 10% foetal bovine serum and 1% penicillin-streptomycin (αMEM, Invitrogen, Thermo Fisher Scientific). RAW264.7 cells were seeded in a concentration of 5000 cells/cm^2 on 96-well plates with α-minimum essential medium with 10% foetal bovine serum and 1% penicillin-streptomycin (αMEM, Invitrogen, Thermo Fisher Scientific Inc. USA). After cell adherence, MC3T3-E1 cells medium was replaced by αMEM with 50 mg/mL ascorbic acid (Sigma-Aldrich, USA), 10 mM ß-glycerol-2-phosphate (Sigma-Aldrich, USA), and part of the RAW264.7 cells was incubated in the presence of 50 ng/mL of Receptor Activator for Nuclear Factor κ B Ligand (RANKL) (R&D Systems, Bio-Techne, Madrid, Spain) to promote osteoclast differentiation. All types of cells (MC3T3-E1, RAW264.7 and RAW264.7 osteoclast precursors) cells were treated with 31.25 and 62.5 µg/mL of AG+CO-coated MX-loaded MSNs (n=8 per concentration). Non-treated cells incubated only with growth medium were considered as control ($n = 8$). All growth media were refreshed every 48 h. These MSNs concentrations were chosen based on the microbiological susceptibility results. Cytotoxicity was tested by CytoTox 96® NonRadioactive Cytotoxicity Assay (Promega, USA) after 48 h of incubation, according to previously published methodology [52]. Cell proliferation was determined by addition of alamarBlue® solution (BIO-RAD, USA) at 10% (v/v) to the cell culture at 14 and 21 days of culture for MC3T3-E1 [53] cells or 4 days for RAW cells [54,55]. The 14-days and 21-days incubations of MC3T3-E1 allow to emulate how the cell proliferation of this type of cells would be affected upon incubation with the nanosystem as it would theoretically take place *in vivo*. Data were represented as relative proliferation of each treatment compared to the control, which was considered as 100% of cell proliferation.

2.6. Hepatotoxicity model

Seven 7-week-old male RjHan:SD - Sprague Dawley rats (Janvier Labs, Le Genest-Saint-Isle, France) were used for primary hepatocytes and Kupffer cells (KCs) isolation as previously described [56,57]. First, the liver was perfused in situ with 200 mL of Hanks' balanced saline solution (HBSS) without Ca^{2+} and Mg^{2+} (Thermo Fisher Scientific) at 10 ml/min and 37 °C without recirculation. The organ was then excised and inserted into a sterile plastic bag where ex situ perfusion was continued with 60 mL of 0.2% pronase (Merck, New Jersey, United States) in HBSS accompanied by 225 mL of 0.01% collagenase (Boehringer-Mannheim, Ingelheim, Germany) in HBSS under the same conditions. The liver was then separated from the perfusion device, the capsule was taken off and the tissue was divided into very small pieces. Tissue was dissociated in a mixture containing 0.03% pronase and 0.01% DNAse in 100 mL of HBSS and was incubated at 37 °C with constant shaking for 30 min. Subsequently, a 125 µm nylon mesh filter was used to filter the liver homogenate removing the undigested tissue. The obtained cell suspension was centrifuged at 70 × g at 4 °C for 4 min. Mature hepatocytes (H) were found in the pellet while non-parenchymal cells (NPCs) were detected in the supernatant. The centrifugations were repeated two more times, and all the supernatants were collected for KCs isolation. To purify the hepatocyte population, the pellets were treated with a Percoll density-gradient centrifugation (GE Healthcare, Marlborough, MA). For KCs isolation, supernatants were treated with 100 mL of HBSS supplemented with 100 µg/mL DNAse and 1% BSA, achieving their dissociation by gently shaking for 5 minutes. The cell suspension was then filtered using a 297 µm nylon mesh filter and centrifuged at 500 × g for 6 min at 4 °C. To separate the KCs from other NPCs cells, the suspension was subjected to an Optiprep density gradient (Sigma-Aldrich, Missouri, United States) and centrifuged at 1400 g for 17 min at 4 °C, thus isolating the KCs.

These cell co-cultures were seeded at a 2:1 ratio (H: KC) on 48-well Type-I collagen-coated plates. First, 375,000 hepatocyte cells were plated into each well and allowed to adhere for approximately 1h at 37 °C / 5% CO_2 with gentle shaking every 20 min. The medium was changed after hepatocytes attachment to remove unbound cells. Then, 187,500 KCs from the same donor-matched were added to each well and again the KCs were allowed to adhere for 1 h, with manual gentle shaking every 20 min. Afterward, the medium of the wells was changed for maintenance and later use. The cells were incubated with two different concentrations of AG+CO-coated MX-loaded MSNs (32.25 and 62.5 µg/mL) for 1 h. Cells incubated with 50 µM of trovaflaxacin (TVX) (Sigma Aldrich, Missouri, United States) plus 1 µg/mL lipopolysaccharide (LPS) (Sigma Aldrich, Missouri, United States) were used as positive control. The supernatant of each condition was then collected and stored at -80 °C until the time of analysis. The levels of each cytokine were measured using rat TNF-α and IL-6 ELISA kits according to the manufacturer's recommendations (Life Technologies, Thermo Fisher Scientific, Massachustts, United States) and quantified using a Synergy^{TM} HTX Multi-Mode Microplate Reader (Biotek,

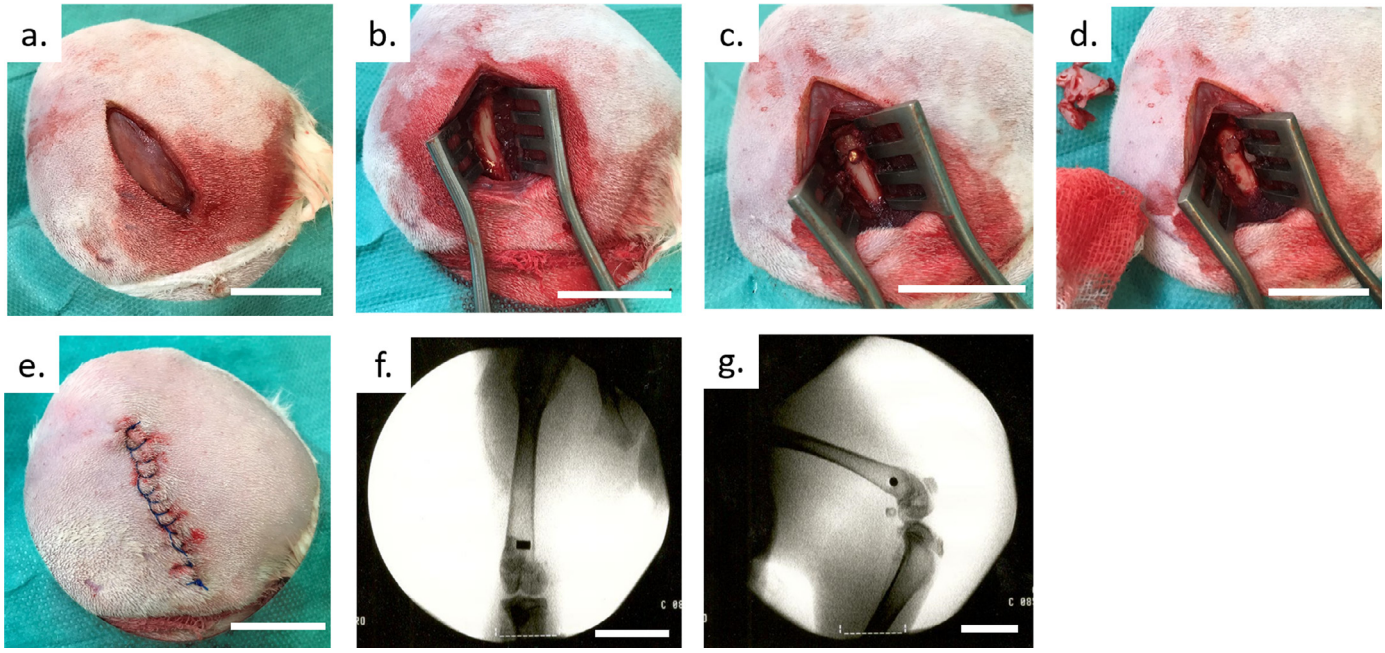

Fig. 1. Surgical model. Skin and muscles were sectioned until the lateral epicondyle was reached (Fig. 1a and b). A hole 3.2 mm in diameter was drilled and cylindrical Ti-6Al-4V implant infected with *E. coli* ATCC25922GFP was placed (Fig. 1c). The infected implant was placed in the bone marrow; the hole was closed with bone wax (Fig. 1d). The wound was closed with a continuous cross suture (Fig. 1e). The correct location of the implant was corroborated through dorsoventral (Fig. 1f) and lateral (Fig. 1g) fluoroscopy of each animal. The white bars represent approximately 2 cm.

Fig. 2. AG+CO-coated MX-loaded MSNs intraosseous treatment. Under general anaesthesia, the femur of each rabbit from the treated group was drilled with a with a 1.5 cm needle (a). The vacuum was made on the needle using drops of sterile serum (b). Finally, 4 mL of 62.5 µg/mL of AG+CO-coated MX-loaded MSNs were injected.

Vermont, USA). CYP3A activity was measured directly in cells in each well by using the P450-Glo ™ CYP3A4 assay with Luciferin-IPA (Promega, Wisconsin, United States) according to the indications for cultured cells, and using a luciferin standard curve (Luciferin Beetle, Promega). Samples were analyzed using a Synergy™ HTX Multi-Mode Microplate Reader.

2.7. In vivo *model*

This study was approved by the Instituto de Investigación Sanitaria of Fundación Jiménez Díaz (IIS-FJD) Animal Care and Use Committee, which includes ad hoc members for ethical issues. Animal care and maintenance complied with institutional guidelines as defined in national and international laws and policies (Spanish Royal Decree 53/2013, authorization reference PROEX109.7/21 July 18, 2021, by the Ministry of the Environment, Local Administration and Territorial Planning of the Community of Madrid and, Directive 2010/63/EU of the European Parliament and of the Council of September 22, 2010).

Specific pathogen free New Zealand white male rabbits (Granja San Bernardo, Navarra, Spain) of between 2.5 and 3 Kg of weight were used. All animals were housed in individual cages in an air-conditioned room at 22 ± 2 °C and light-darkness cycles of 12:12 h.

2.7.1. *Evaluation of systemic administration*

Three rabbits were treated under general anaesthesia with an intravenous injection through the marginal vein of the left ear of 62.5 µg of AG+CO-coated MX-loaded MSNs per millilitre of rabbit blood, considering that each animal possesses 66.33 mL of blood per kilogram [58]. Two days after the intravenous treatment, each animal was euthanized under general anaesthesia by intracardiac overdose of sodium thiobarbital. The rabbit spleen, liver and a kidney were recovered through sterile preparation, surgical field isolation. All organs were fixed, paraffin-infiltrated, and haematoxylin-eosin stained.

2.7.2. *Osteomyelitis model*

The *E. coli* ATCC25923-GFP strain was employed for this *in vivo* model. Each animal was placed in the supine position under general anaesthesia, its right hind leg was immobilised and isolated in a sterile field. Skin and muscles were sectioned until the lateral epicondyle was reached (Fig. 1a and b). A hole 3.2 mm in diameter and 1 cm deep was drilled. A 5 mm-long and 3 mm-diameter cylindrical Ti-6Al-4V implant infected with *E. coli* was placed (Fig. 1c). Each implant was incubated with 2 mL of a 3 McFarland suspension of *E. coli* in saline (≈2.58×10^8 colony-forming units per millilitre) in a well from a 12-well plate for 2 h at 37 °C and 5% CO_2 for implant infection. After incubation, each implant

was washed with 2 mL of saline (B. Braun, Germany). After lodging the infected implant in the bone marrow, the hole was closed with Ethicon bone wax (Johnson & Johnson, United States) (Fig. 1d). The entire area was disinfected with 6-volume hydrogen peroxide. The wound was closed with a continuous cross suture using a 3/0 Prolene suture (Johnson & Johnson, United States) (Fig. 1e). The correct location of the implant was corroborated through dorsoventral (Fig. 1f) and lateral (Fig. 1g) fluoroscopy of each animal. The behavior, temperature and weight of each animal were monitored every 24 h throughout the experimental procedure.

The infected animals were randomly assigned to two groups, namely control group ($n = 3$) and AG+CO-coated MX-loaded MSNs treated group ($n = 3$). The sample size was estimated by Wilcoxon Mann-Whitney test and an a-priori type of power analysis considering $d = 4.00$, $\alpha = 0.05$, $(1\text{-}\beta) = 0.95$, allocation ratio = 1 by using G*Power 3.1.9.7 software [59]. The d parameter assumes that AG+CO-coated MX-loaded MSNs treatment can reduce the bacterial concentration by at least 99% per gram of bone when compared to the uncoated implant group. The statistical power of the sample was 0.983.

Three days after the surgery, each animal was anaesthetized and treated with a 4 mL intraosseous injection of 62.5 µg/mL of AG+CO-coated MX-loaded MSNs by using a 1.5 cm needle and Arrow® EZ-IO® Intraosseous Vascular Access System (Teleplex, Ireland) (Fig. 2). The control group received no treatment. Two days after the intraosseous treatment, all animals were euthanized under general anesthesia by intracardiac overdose of sodium thiobarbital. The rabbit femur, liver and a kidney were recovered through sterile preparation.

For microbiological studies, each femur with the implant was smashed with a hammer. This smash was immersed in sterile saline and sonicated using an Ultrasons-H 3000840 low-power bath sonicator (J. P. Selecta, Barcelona, Spain) at 22 °C for 5 min [50]. The resulting sonicate was diluted in a 10-fold dilution bank and seeded on blood-chocolate agar (Biomérieux, Marcy-l'Étoile, France) using the spread plate method [60,61]. The concentration of bacteria was estimated as CFU/g of bone and adnexa. The liver and one kidney of each animal were intended for pathological studies. Histological sections were fixed, paraffin-infiltrated, and hematoxylin-eosin stained.

2.8. Statistical analysis

Statistical analyses were performed using Stata Statistical Software, Release 11 (StataCorp 2009). Data were evaluated using a one-sided Wilcoxon nonparametric test to compare two groups. Statistical significance was set at p-values ≤ 0.05. All results are represented as median and interquartile range.

3. Results

3.1. Nanoparticles characterization

3.1.1. Synthesis and functionalization of mesoporous silica nanoparticles

The successful coating with AG and CO was confirmed through different characterization techniques (Figs. 3 and S2). TGA (Fig. 3a) showed a difference in a weight loss of 8% and 14% for AG-coated

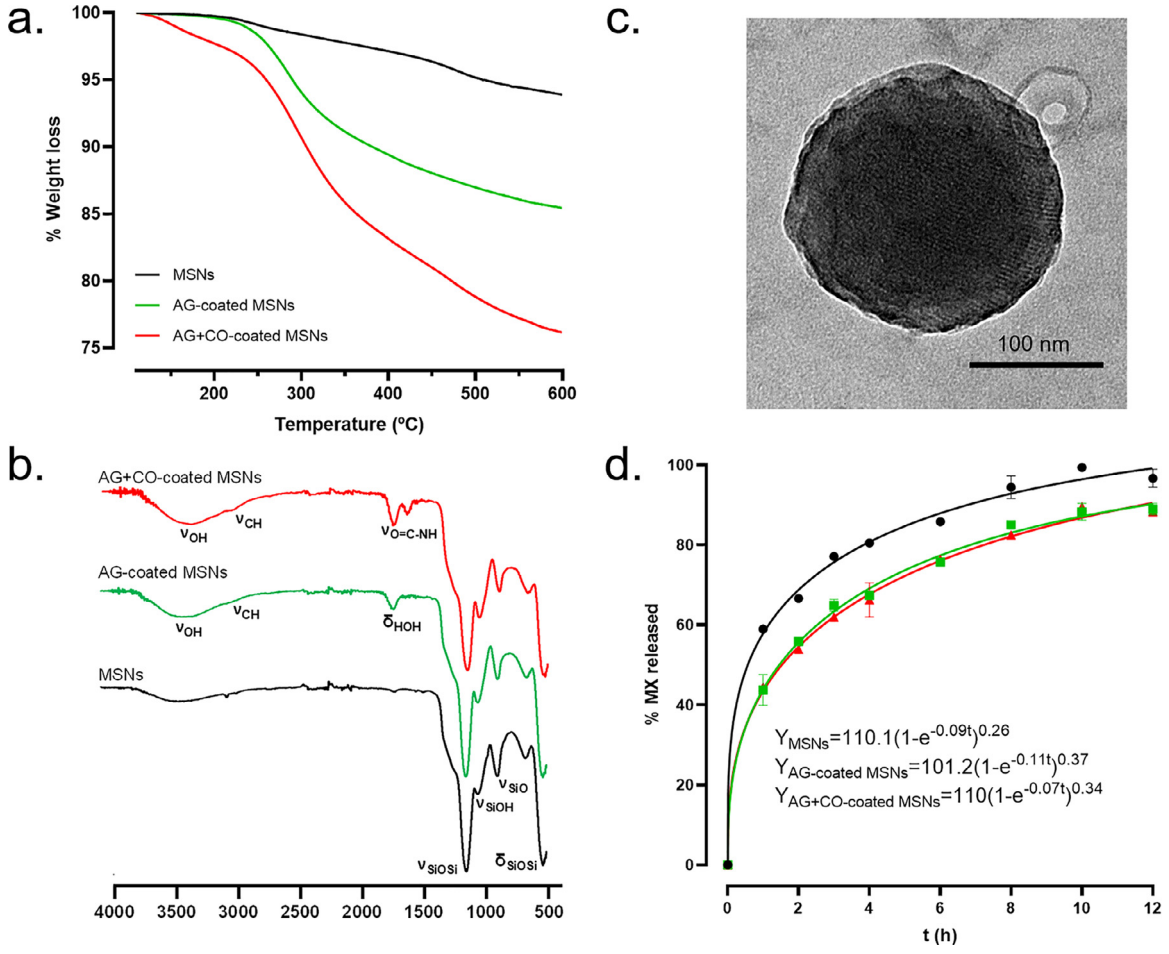

Fig. 3. Physico-chemical characterization of the different nanoparticles. (a) Thermogravimetric analysis, (b) FTIR spectroscopy, (c) TEM image of phosphotungstic acid-stained AG+CO-coated MSNs, (d) MX release experiment from MSNs (black), AG-coated MSNs (green) and AG+CO-coated MSNs (red), (e) CO-FITC release experiment from CO-coated MSNs (black) and AG+CO-coated MSNs (red) (For interpretation of the references to color in this figure legend, the reader is referred to the web version of this article).

MSNs and AG+CO-coated MSNs, respectively, compared to pristine MSNs. Hence, it could be concluded that the amount of CO adsorbed onto the surface was *ca.* 6%. The presence of AG and CO was further confirmed through FTIR spectroscopy (Fig. 3b). In this regard, the appearance of a deep vibration band at *ca.*3400 cm^{-1} (ν_{OH}) as well as a subtle one at *ca.*3,000 cm^{-1} (ν_{CH}) in the AG-coated MSNs spectrum were ascribed to the presence of AG. This was in agreement with the vibration bands observed for AG alone (Fig. S3). Finally, the presence of vibrations bands at 1650 and 1,540 cm^{-1} that were ascribed to the amide bonds of CO undoubtedly confirmed its successful adsorption onto the surface. Besides, AG+CO-coated MSNs were stained with phosphotungstic acid and observed under the TEM, where the blurry surface was indicative of organic matter deposition (Fig. 3c). Zeta potential measurements on AG+CO-coated MSNs yielded a value of -21.6 mV, which was less negative than what observed for MSNs (-34.8 mV), in agreement with the presence of free amino groups throughout the structure of CO. Finally, the colloidal stability of different nanoparticles was analysed through DLS measurements, yielding a size distribution centred at 190 nm (Fig. S2). In this sense, the stability of nanoparticles remained unaffected by different functionalizations, highlighting their suitability for biomedical applications.

3.1.2. Antibiotic release from MSNs

MX release from the different nanomaterials was evaluated in vial. As shown in Fig. 3d, modifying the surface with a macromolecule with affinity for the biofilm, AG, and a high molecular weight antibiotic, CO, led to release kinetics similar to that observed for MSNs. The different release data shown in Fig. 3d were fitted to a first-order kinetic model with an empirical nonideality

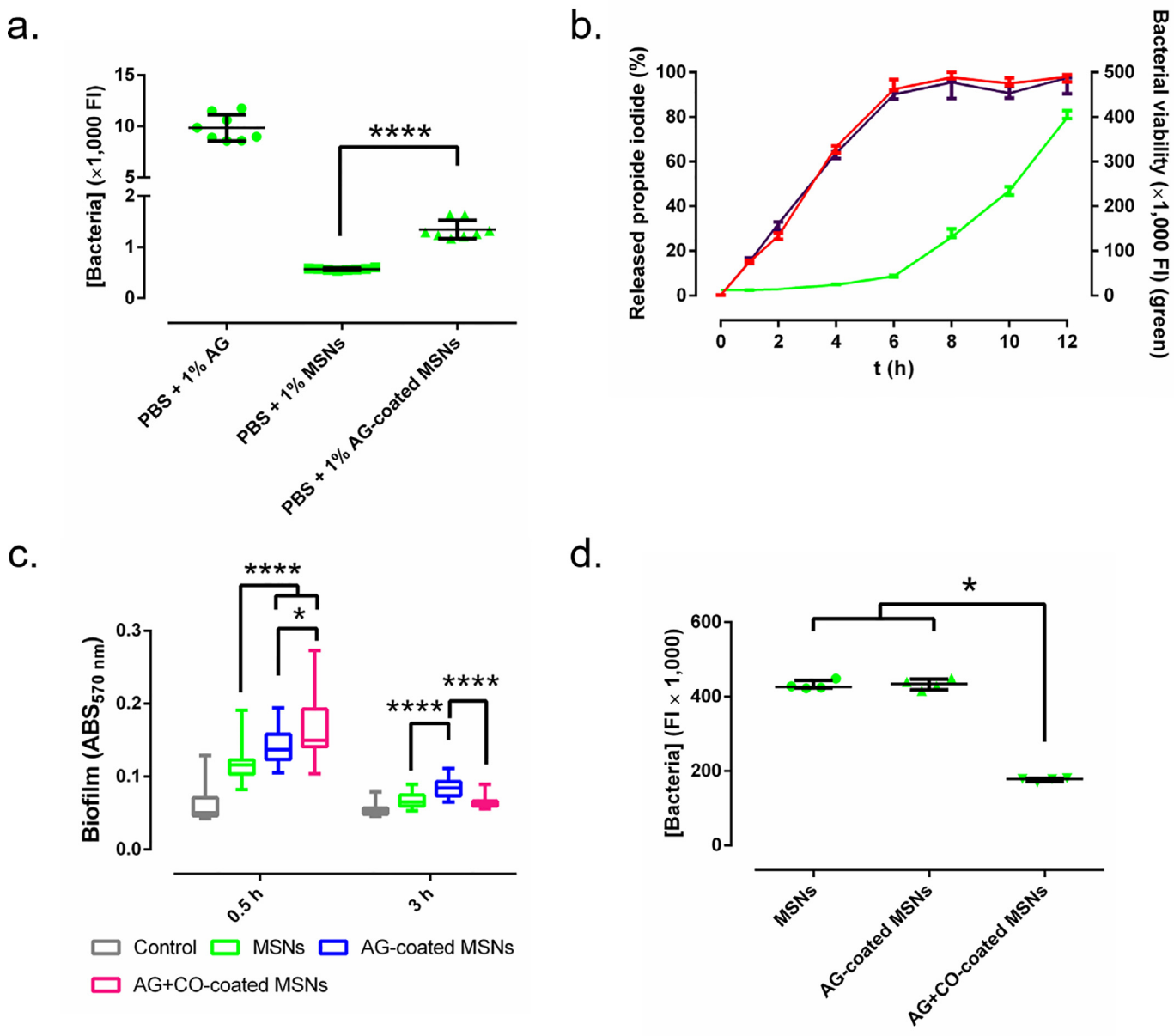

Fig. 4. *E. coli*-AG-coated MSNs interaction. (a) Use of AG-coated MSNs by *E. coli* as a carbon source. (b) Propidium iodide release from MSNs (red) and AG-coated-MSNs (purple) in presence of *E. coli* that is actively replicating (green). (c) *E. coli* biofilm- AG-coated MSNs interaction. (d) *E. coli* planktonic cells-AG-coated MSNs interaction. FI: fluorescence intensity. *: p-value < 0.05, ****: p-value < 0.0001 for Wilcoxon test (For interpretation of the references to color in this figure legend, the reader is referred to the web version of this article).

factor (δ) (Eq. (1)) [62,63]:

$$Y = A\left(1 - e^{-kt}\right)^{\delta} \quad (1)$$

Where Y is the percentage of MX released at time t, A the maximum amount of MX released (in percentage), and k, the release rate constant. The obtained values are summarized in Fig. 3d.

On the other hand, the release profile of CO-FITC+AG-coated MSNs (Fig. 3e) demonstrated that the AG coating enhanced the amount of CO loaded onto the surface, which could be beneficial for the biological studies, as it would reduce the need to use high doses of this nanomedicine.

3.2. Microbiological studies

3.2.1. Bacteria-nanoparticle interaction

AG-coated MSNs were incubated with *E. coli* to evaluate whether the polymeric coating could be effectively degraded into its monomers by such enzymes and be employed as a carbon source by the bacteria. As shown in Fig. 4a, *E. coli* concentration showed more than two-fold increase in the presence of AG-coated MSNs compared to pristine MSNs (p-value < 0.0001). The enzymatic degradation of AG was further confirmed through a release experiment. For that purpose, MSNs and AG-coated MSNs were placed with bacteria to evaluate whether the enzyme-mediated degradation of AG affected the release profile (Fig. 4b). In contrast to Fig. 1d, the PI release was almost equal from MSNs and AG-coated MSNs in presence of *E. coli*. The different nanoparticles were then faced to an *E. coli* mature biofilm and left to interact for 30 min. As observed in Fig. 4c, the highest retention values were observed for both AG- and AG+CO-coated MSNs, showing the latter slightly more accumulation ($p < 0.0307$). However, the analysis of the interaction at 3 h demonstrated that AG-coated MSNs maintained its high retention capability, whereas that of AG+CO-coated MSNs significantly decreased, equalling the results obtained for pristine MSNs.

AG+CO-coated MSNs significantly reduced the *E. coli* viability (p-value $= 0.0143$) compared to AG-coated MSNs and pristine MSNs (by 42% and 41%, respectively) (Fig. 4d). These results were confirmed by using TEM (Fig. 5), which allowed to inspect visually the physical changes induced by the drug-loaded nanoparticles on the bacteria. Bacteria faced to pristine MSNs and AG-coated MSNs showed a normal appearance, with an intact outer membrane and bacterial wall intimately linked to the cytoplasm (Fig. 5a–d). In some cases, AG-coated MSNs were intimately in contact with the outer membrane of some bacteria (Fig. 5d). The interaction between *E. coli* and AG+CO-coated MSNs gave rise to the presence of vacuoles inside the bacteria (Fig. 5e and f) resulting from the detachment of the cytoplasmic membrane from the cell wall right where the bacterium had interacted with an AG+CO-coated MSN, which was unequivocally ascribed to bacterial death (Fig. 5f).

3.2.2. Minimal inhibitory concentration (MIC), minimal bactericidal concentration (MBC), minimal biofilm inhibitory concentration (MBIC), and minimal biofilm eradication concentration (MBEC)

The antibacterial effect of the nanoparticles was evaluated by studying the MIC and MBC. For that purpose, different nanoparticles were faced against planktonic *E. coli* at different concentrations. The MIC and MBC of MX against *E. coli* were found to be $<$ 0.0625 μg/mL for both. The MIC and MBC of CO against *E. coli* were found to be 2 μg/mL for both. The MIC and MBC of MX-loaded MSNs against *E. coli* were found to be $<$1.953 μg/mL for both. The MIC and MBC of CO-coated MSNs against *E. coli* were found to be 15.625 μg/mL for both. Finally, the MIC and MBC of AG+CO-coated MX-loaded MSNs against *E. coli* were found to be 1.953 and 3.906 μg/mL, respectively.

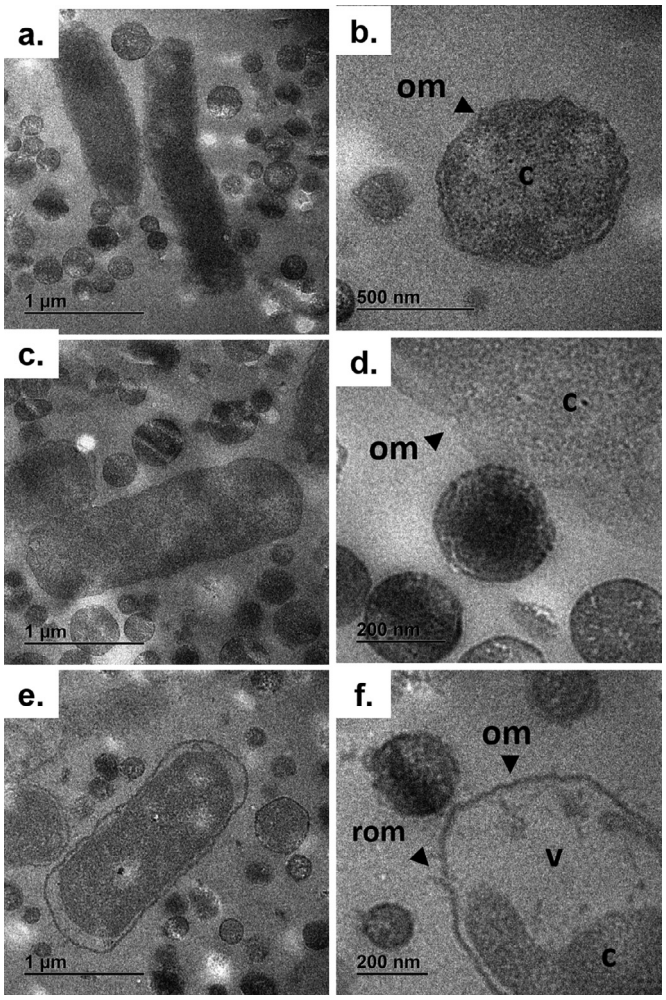

Fig. 5. TEM images of *E. coli* planktonic cells faced to MSNs (a and b), AG-coated MSNs (c and d), and AG+CO-coated MSNs (e and f). C: cytoplasm. OM: outer membrane. ROM: ruptured outer membrane. V: vacuole.

The antibiofilm effect of nanoparticles was evaluated by studying the MBIC and MBEC. For that, different nanoparticles were faced against an *E. coli* biofilm at different concentrations. The MBIC and MBEC of MX against *E. coli* was found to be $<$0.0625 and 1 μg/mL, respectively. The MBIC and MBEC of CO against *E. coli* were found to be 64 and 128 μg/mL, respectively. The MBIC and MBEC of MX-loaded MSNs against *E. coli* were found to be 1.953 and 15.625 μg/mL, respectively. The MBIC and MBEC of AG+CO-coated MSNs against *E. coli* were found to be 2,000 and $>$2,000 μg/mL, respectively. Finally, the MBIC and MBEC of AG+CO-coated MX-loaded MSNs against *E. coli* were found to be 1.953 and 7.813 $\mu g/mL$, respectively.

Bearing in mind the above-described results, and an *in vitro* model of infected bone was developed for the subsequent preparation of *in vivo* experiment. For that purpose, two concentrations of AG+CO-coated MX-loaded MSNs, 31.25 (4 × MBEC) and 62.5 μg/mL (8 × MBEC), were chosen to be used against *E. coli*. Both concentrations of AG+CO-coated MX-loaded MSNs were able to decrease more than 99.9% the viability of biofilm grown on the trabecular bone compared to non-treated biofilm (p-value < 0.01) (Fig. 6a). Furthermore, the 62.5 μg/mL concentration significantly reduced 98.9% more bacteria than 31.25 μg/mL concentration (p-value $= 0.0238$). To support these numerical results, representative images from each treatment were taken (Fig. 6b–i). Non-treated *E. coli* biofilm showed many different small viable aggre-

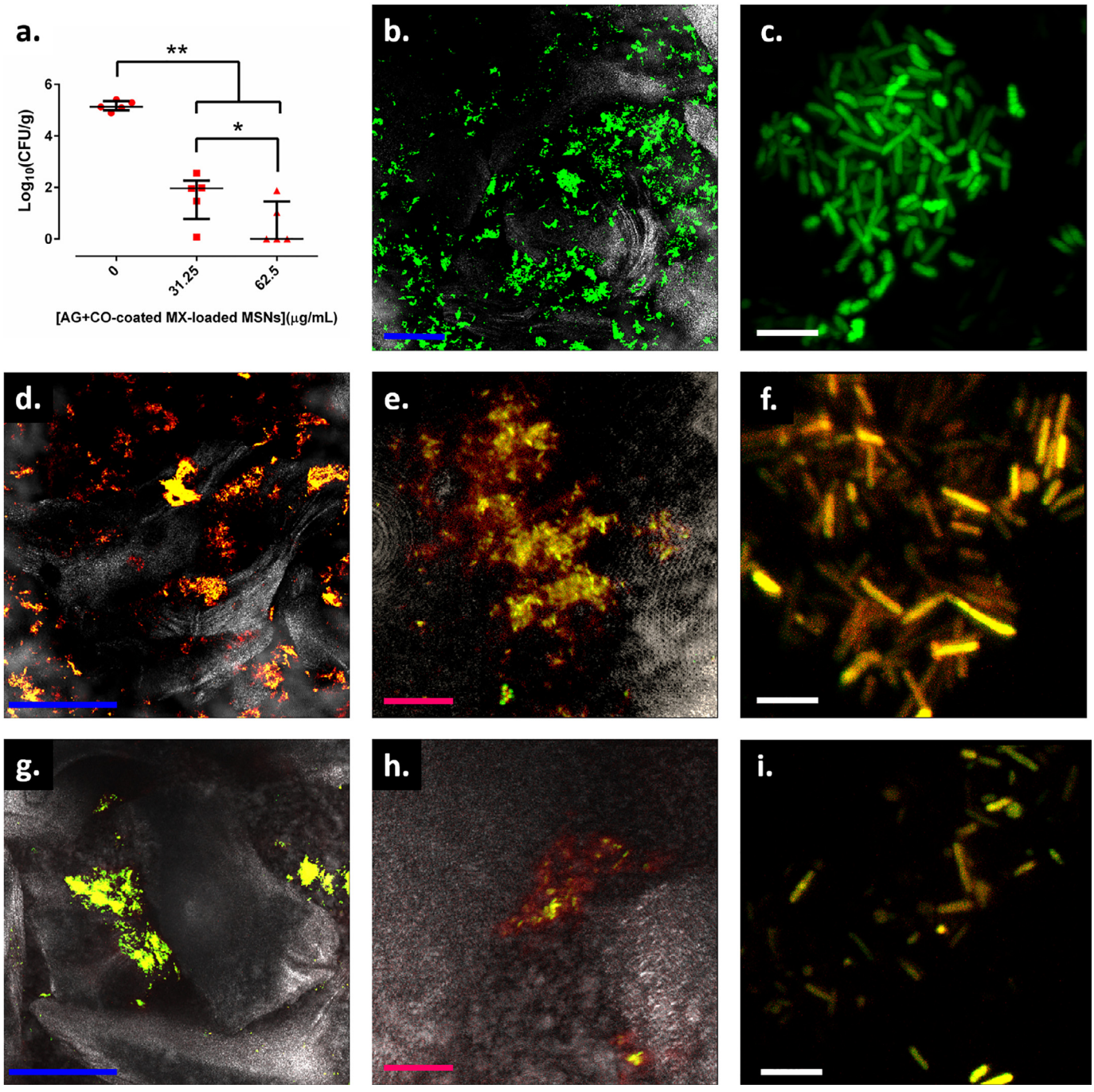

Fig. 6. Bacterial quantity per gram of trabecular bone after 24 h treatment with each AG+CO-coated MX-coated MSNs (a). Representative confocal images from the different conditions: (b and c) positive control, (d, e and f) 31.25 μg/mL, and (g, h and i) 62.5 μg/mL of AG+CO-coated MX-coated MSNs. Green represents the *E. coli* viable bacteria, red represent the AG+CO-coated MX-coated MSNs, and grey represent the trabecular bone surface. *: p-value < 0.05, **: p-value < 0.01 for Wilcoxon test. Blue, pink and white bars represent 250, 25, and 7.5 μm, respectively (For interpretation of the references to color in this figure legend, the reader is referred to the web version of this article).

gates of bacteria or microcolonies mainly adhered on the bone surface (Fig. 6b and c), an aspect that is reminiscent of the microscopic appearance of certain biofilms isolated from clinical samples [64]. When *E. coli* biofilm was exposed to 31.25 μg/mL, the number of aggregates was slightly lower (Fig. 6d–f). In this case, AG+CO-coated MX-loaded MSNs adhered on microcolonies. This MSNs attachment would be responsible for the absence of viable bacteria (absence of green fluorescence) in the periphery of microcolonies (Fig. 6d–f). The best results were obtained when the *E. coli* biofilm was treated with 62.5 μg/mL of AG+CO-coated MX-loaded MSNs (Fig. 6g and h). As shown in Fig. 4g, the quantity of viable bacteria into the microcolonies adhered on the bone surface was extremely scarce. Likewise, AG+CO-coated MX-loaded MSNs adhered on those few aggregates, but the viable bacteria inside of them were fewer than those in the microcolonies treated with 31.25 μg/mL (Fig. 6h and i). At microscopic level (Fig. 7), untreated *E. coli* biofilm grown on bone showed bacterial clusters adhered on bone and was embedded in exopolymeric substances (Fig. 7a–c), in opposition to the *E. coli* cells observed on the bone surface treated with 32.5 and 61.25 μg/mL (Fig. 7d–f) which were found in the form of aggregates, mainly 32.5 μg/mL, or simply as individualized cells completely covered by the nanoparticles

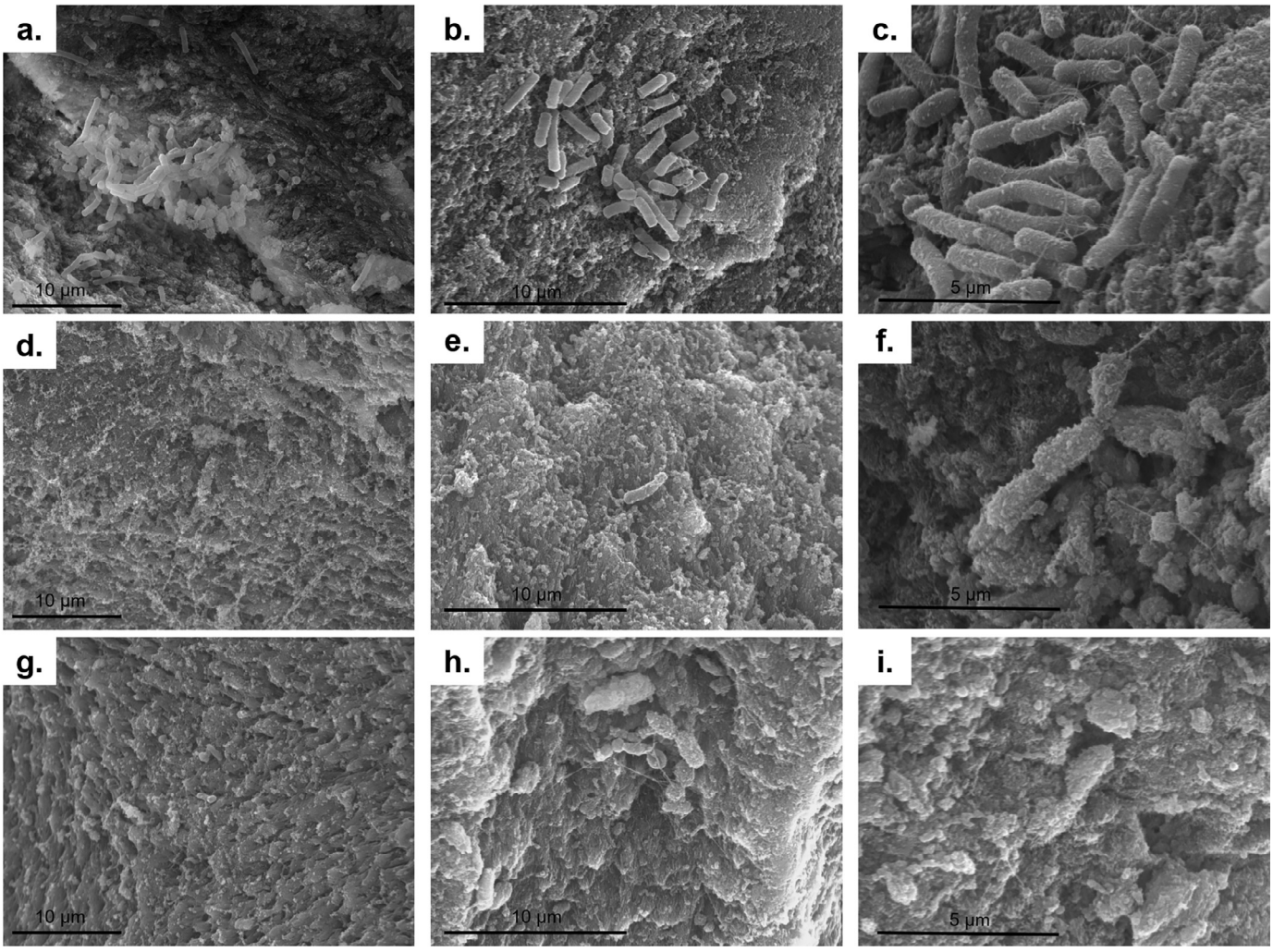

Fig. 7. SEM images of *E. coli* biofilm grown on trabecular bone after 24 h treatment with each AG+CO-coated MX-coated MSNs: (a, b andc) positive control, (d, e andf) 31.25 µg/mL, and (g, h, and i) 62.5 µg/mL of AG+CO-coated MX-coated MSNs.

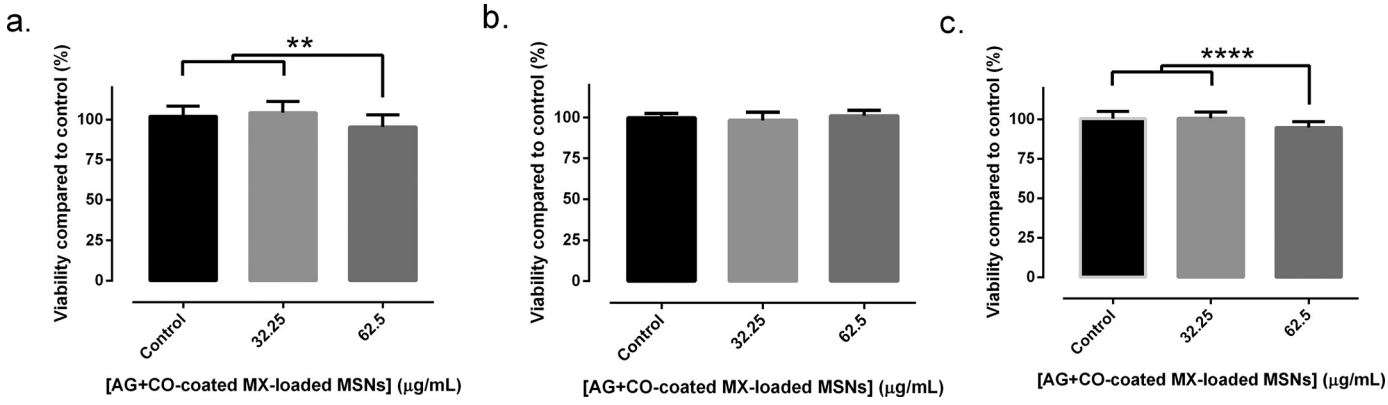

Fig. 8. Cytotoxicity of AG+CO-coated MX-coated MSNs concentration on MC3T3-E1 osteoblasts (a), RAW264.7 osteoclasts (b), and RAW264.7 macrophages (c). **: *p*-value < 0.01, ****: *p*-value < 0.0001 for Wilcoxon test.

and displaying important membrane damages, mainly 61.25 µg/mL (Fig. 7g-i).

3.3. Cell studies

The biocompatibility of AG+CO-coated MX-loaded MSNs was evaluated on bone-related cells (Fig. 8). AG+CO-coated MX-loaded were found to be non-cytotoxic for osteoclasts, and only reduced cytotoxicity was observed at the highest concentration (62.5 µg/mL) for osteoblasts and macrophages. Moreover, AG+CO-coated MX-loaded MSNs had an impact on the cell proliferation of osteoblast and macrophages (Fig. 9a, c), since these cells decreased their proliferation in presence of nanoparticles. Interestingly, osteoblast showed a dose-dependent effect on proliferation at 14 days, but these cells showed better proliferation in presence of 62.5 µg/mL than 31.25 µg/mL at 21 days (Fig. 9a).

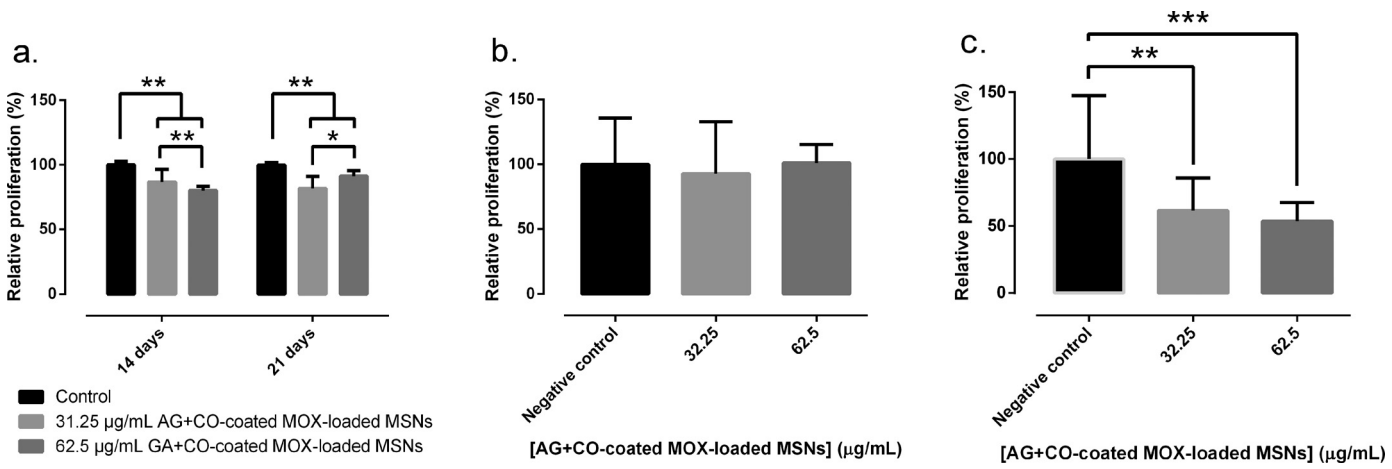

Fig. 9. Cell proliferation of MC3T3-E1 osteoblasts (a), RAW264.7 osteoclasts (b), and RAW264.7 macrophages (c) in presence of each AG+CO-coated MX-loaded MSNs concentration. *: p-value < 0.05, **: p-value < 0.01, ***: p-value < 0.001 for Wilcoxon test.

3.4. Hepatotoxicity model

The results derived from the hepatotoxicity model are shown in Fig. 10. Tumor necrosis factor-α (TNF-α) increased proportionally with the concentration of AG+CO-loaded MX-loaded MSNs (Fig. 10a), whereas interleukin-6 (IL-6) showed opposite behavior (Fig. 10b). In addition, cytochrome P450 metabolic capacity (CYP3A) decreased proportionally with the concentration of nanoparticles (Fig. 10c).

In vivo studies

3.4.1. Evaluation of systemic administration

The three livers showed a preserved hepatic parenchyma architecture with absence of hepatocyte lesion. In one of the animals, mild intraepithelial lymphocytosis in the ducts and presence of chronic central perivenular inflammatory aggregates were identified. In the remaining two, mild signs of ductulitis were observed, with signs of lymphocytosis in bile ducts (Fig. 11a and b). The three kidneys showed a renal parenchyma with normal morphology and appearance without glomerular or tubular lesions, and absence of inflammation or necrosis (Fig. 11c and d). The three spleens showed a splenic pulp without relevant microscopic alterations (Fig. 11e and f).

3.4.2. Osteomyelitis model

AG+CO-coated MX-loaded MSNs completely eradicated E. coli infection in two out of the three treated femurs and reduced up to 99.4% in the remaining femur, compared to the control group (Fig. 12).

The three livers of control (untreated) group showed liver parenchyma with mild-moderate central perivenous portal inflammation and minimal lobular hepatitis (Fig. 13a and b). The inflammatory infiltrate consisted of lymphocytes, plasma cells and eosinophils (Fig. 13c). The livers of AG+CO-coated MX-loaded MSNs-treated group showed liver parenchyma with preserved cytoarchitecture without hepatocyte lesions (Fig. 13d). Minimal foci of ductulitis with signs of lymphocytes in bile ducts were observed in all three treated animals (Fig. 13e and f). Focal signs of cholestasis were detected in one of the treated rabbits. All the kidneys from both control group and AG+CO-coated MX-loaded MSNs-treated showed renal parenchyma of normal morphology and appearance without glomerular or tubular lesions, and absence of inflammation or necrosis.

4. Discussion

In this study, we demonstrate the feasibility of using AG+CO-coated MX-loaded nanoparticles to treat bone infections caused by *E. coli*, showing no cytotoxicity on osteoblast, osteoclast and macrophages *in vitro*, and absence of organ damage *in vivo* upon intraosseous administration.

Given the bacterial origin of this kind of infection, two clinically relevant antibiotics, MX and CO, were selected as cargos. Because of its low molecular weight (401 g/mol), MX would be easily loaded within the mesoporous of nanoparticles, as previously reported [65,66]. Conversely, CO would be likely adsorbed onto the surface of nanoparticles, as previously stated for other polymixins and MSNs [32,67,68].

The MX release was monitored and fitted to a first-order kinetic model (Fig. 1d). In this model, the values for δ are comprised between 0, for materials that release the drug at the very beginning of the experiment, and 1, for materials that follow the first-order kinetics. According to Fig. 1d, the δ values estimated for the different nanoparticles were closer to 0, in agreement with the pronounced burst effect observed during the initial hour. This kinetics has also been observed for other antibiotics loaded in mesoporous silica-based nanoparticles [69]. Also, δ_{MSNs} was comparatively lower than those of coated samples, which would account for the slight differences observed among them during release experiments. Considering these results, the AG+CO-coated MSNs would be able to release large amounts of MX in a short time, thereby achieving high local concentration of antibiotics nearby bacteria from a low quantity of nanoparticles, which might reduce the potential side effects associated with other administration routes.

Even though CO might have been simply adsorbed on the surface of particles and directly used against bacteria, our results indicate that incorporating CO along with the AG coating was beneficial to enhance the final amount of this antibiotic on nanoparticles (Fig. 1e). We hypothesize that the reason behind this result would be that AG can act as a polymeric mesh that would favour the retention of CO on nanoparticles during the washing steps, resulting in a significantly higher final amount of antibiotic loaded. Hence, although the synergetic effect of the use of polimixins plus another antibiotic has been previously reported [32], this work demonstrates that the use of Arabic gum improves the adsorption capacity of nanoparticles, potentially diminishing the final nanoparticle dose that would be required during the treatment if CO alone was to be used.

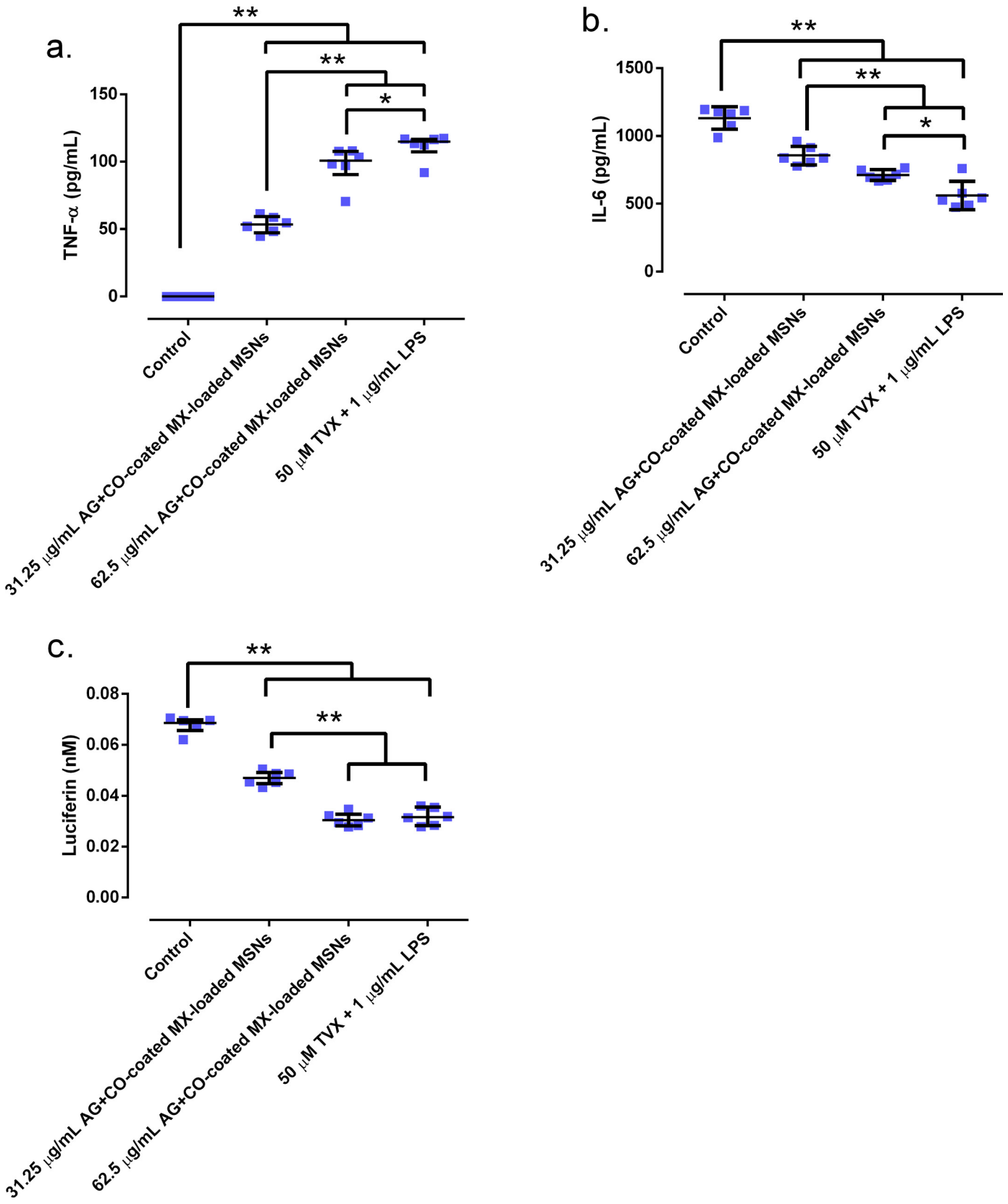

Fig. 10. Tumor necrosis factor α (TNF-α) (a), interleukin 6 (IL-6) (b), and cytochrome 3A metabolic capacity (c) from the rat hepatocyte-Kupffer cells co-cultive. *: p-value < 0.05, **: p-value < 0.01 for Wilcoxon test.

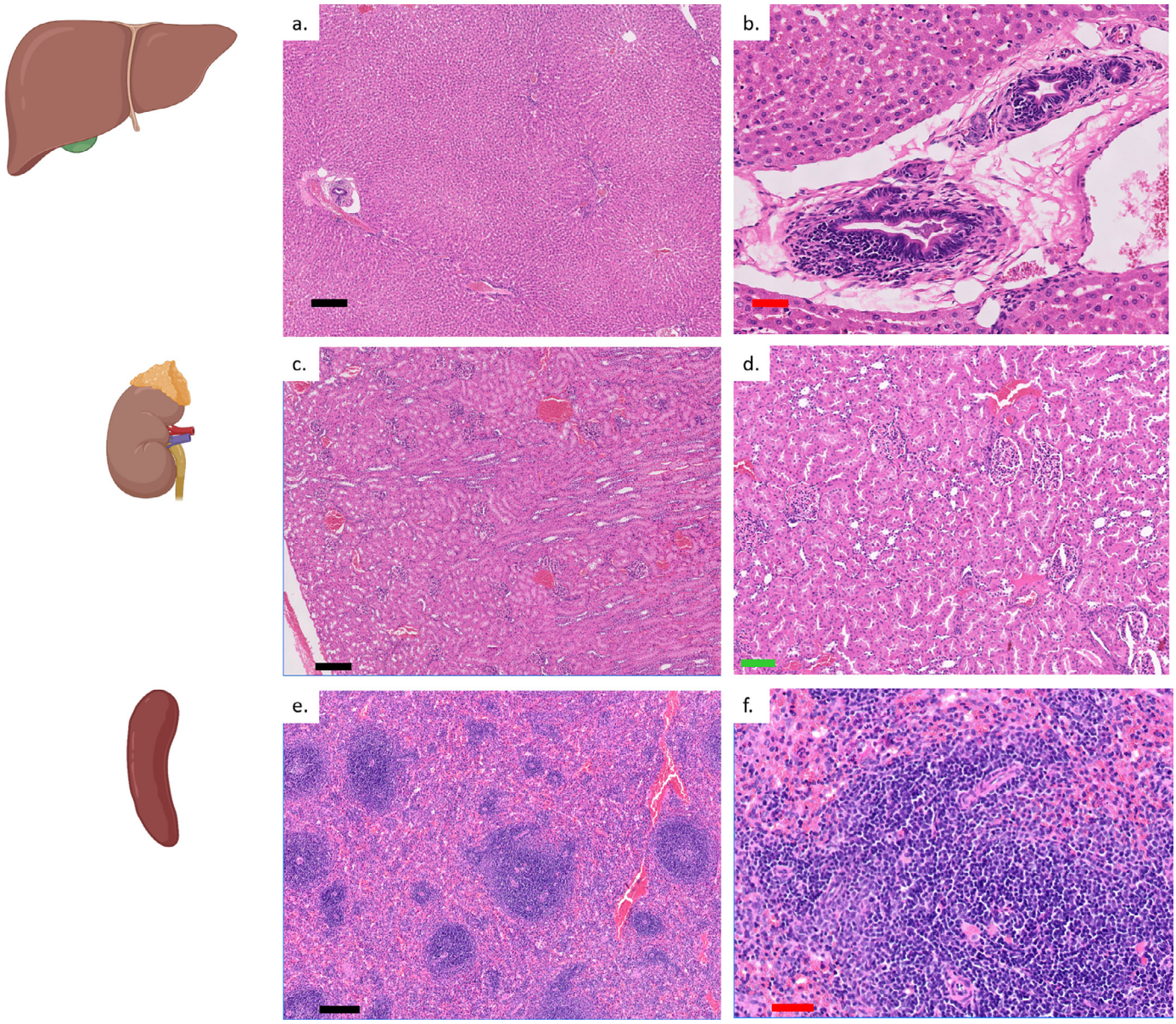

Fig. 11. Histological liver (a, b), kidney (c,d) and spleen (e, f) images with hematoxylin-eosin stain from a rabbit that received systemically one AG+CO-coated MX-loaded MSNs dose. Black, green, and red bars represent 200, 100, and 50 µm, respectively (For interpretation of the references to color in this figure legend, the reader is referred to the web version of this article).

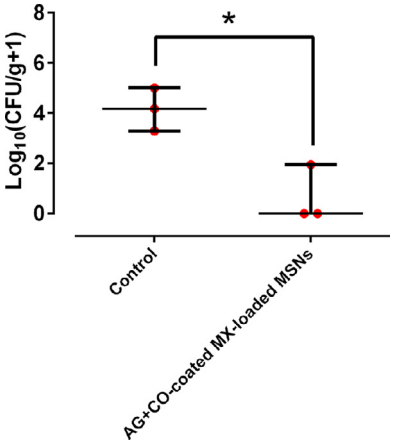

Fig. 12. Quantity of *E. coli* in bone and adnexa. $*p$-value < 0.05 for Wilcoxon test.

AG, a branched-chain, complex polysaccharide composed of 1,3-linked β-D-galactopyranosyl monomers connected to the main chain through 1,6-linkages [27], can be degraded by the enzymatic battery of enterobacteria [70–72]. In this sense, our results (Fig. 2a) confirmed that AG coating can be degraded by *E. coli* enzymes into galactopyranose monomers that are used as a carbon source [30,31]. This finding points out that AG lacks antibacterial capacity *per se*, unlike other gums such as Iranian gum do [73]. That enzymatic degradation of AG was further confirmed through a PI release experiment (Fig. 2b), in which almost equal amount of PI was released from MSNs and AG-coated MSNs in presence of *E. coli*, demonstrating that *E. coli* metabolically active cells can degrade the AG coating while the bacterium grows. The interaction between *E. coli* mature biofilm and different nanoparticles (Fig. 2c) brought out that AG-coated MSNs showed a higher accumulation that non-coated ones at short time (30 min). Interestingly, AG+CO-coated MSNs showed a slight but significantly higher accumulation than AG-coated MSNs. However, setting the incubation period at

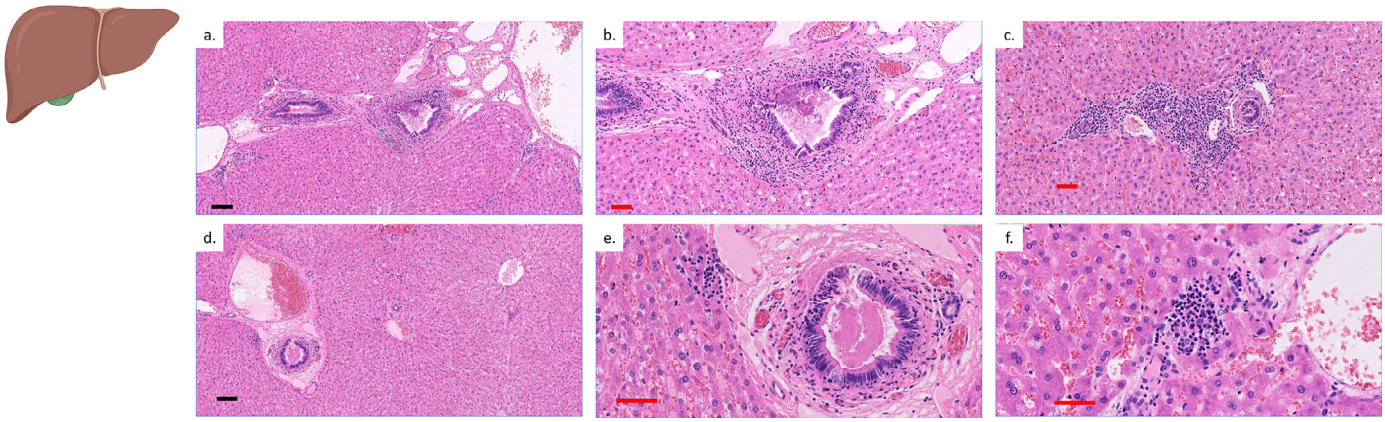

Fig. 13. Histological liver images with hematoxylin-eosin stain of untreated rabbit (a–c) and AG+CO MX-loaded MSNs-treated rabbit (d–f). Black and red bars represent 100 μm, and 50 μm, respectively (For interpretation of the references to color in this figure legend, the reader is referred to the web version of this article).

3 h revealed that AG-coated MSNs maintained its high accumulation capability to biofilm, whereas that of AG+CO-coated MSNs matched that of pristine MSNs. Thus, our results would indicate that functionalizing the surface of MSNs with AG increased the targeting ability of nanoparticles for *E. coli* infectious foci. This enhanced accumulation might be the result of the biomatrix accumulation of enzymes [74] able to cleave the polymeric chains of AG, e.g. β-galactosidase [75]. This enzymatic cleavage would favour the retention of nanoparticles to biofilm matrix at very short times and would made the AG coating a specific coating for *E. coli* and other enterobacteria that secrete these enzymes [76]. After this accumulation, the colistin carried by the AG-coated MSNs would be released and exert a destabilising effect on the *E. coli* biofilm matrix structure [77]. To the best of our knowledge, this is the first study that uses a gum of natural origin as a targeting agent for a specific bacterial pathogen. Overall, gums of different origin are worth being explored as there are already few examples of their potential in nanomedicine. For instance, it has been reported that Guar gum can be used as targeting agent for colorectal cancer treatment [78–81]. Similarly, Iranian gum has been shown to present antimicrobial properties *per se* and has been used for wound healing applications [73]. Besides, these gums have been recently incorporated into hydrogels that show unique advantages compared to other polymeric materials, and find application as periodontal materials, drug carriers, bone matrices [82–85], and artificial blood vessels fabricated by 3D printing [86]. Some of those hydrogels, as those composed of Arabic gum, gelatin plus polyurethane [87], or those containing N–O–carboxymethyl chitosan [88] have been also used for wound healing applications and wound infection prevention.

It is known that CO kills Gram-negative bacteria throughout five mechanisms: (1) disruption of the bacterial outer and inner membranes, (2) vesicle-vesicle contact pathway, (3) hydroxyl radical death pathway, (4) inhibition of respiratory enzymes, and (5) anti-endotoxin colistin activity [89]. Any of these mechanisms would be responsible for the bactericidal effect observed in AG+CO-coated MSNs at short term (30 min) against the planktonic state of *E. coli*. These results were further supported by TEM study, where the presence of vacuoles resulting from the detachment of the cytoplasmic membrane from the cell wall and outer membrane [90] was only detected in the bacteria exposed to AG+CO-coated MSNs.

The antibacterial effect of nanoparticles was evaluated by MIC and MBC. According to the results obtained, *E. coli* ATCC 25922-GFP is susceptible to MX ($<$ 1 μg/mL) [91] and CO ($\leq$2 μg/mL) [92]. In consequence, the combined use of both antibiotics seems highly appropriate for achieving outstanding therapeutic effect against *E. coli* ATCC25922GFP. On the other hand, the antibiofilm effect of nanoparticles was evaluated by MBIC and MBEC. For that purpose, different nanoparticles were faced against an *E. coli* biofilm at different concentrations, resulting the MBIC and MBEC of AG+CO-coated MX-loaded MSNs against *E. coli* 1.953 and 7.813 μg/mL, respectively. In light of these results, MX would be a possible treatment for *E. coli* biofilm, as recommended by other authors [93,94]. Despite CO was shown to be ineffective in inhibiting and eradicating the *E. coli* biofilm, the actual role of this antibiotic in the potential treatment of osteomyelitis will be discussed later.

Given the promising results, the antibacterial efficacy of AG+CO-coated MX-loaded MSNs in a more realistic scenario was studied by using an *in vitro* model of bacterial biofilm grown in wound-like medium [40,41] on bovine trabecular bone. The highest concentration of AG+CO-coated MX-loaded MSNs (62.5 μg/mL; 8 $\times$ MBEC) was the most effective against *E. coli* biofilm. The main differences between two concentrations were (1) the bacterial viability and (2) the quantity of microcolonies adhered on the bone (Fig. S4). The bacterial viability reduction was a consequence of the MX released from loaded nanoparticles, as this antibiotic is a fourth-generation broad-spectrum fluoroquinolone that is highly effective against biofilm-related infection [95–97]. In addition, this antibiotic is a recent fluoquinolone and has been seldom used in the antibiotic-loaded nanoparticle field, where the main fluoroquinolone used is levofloxacin [98–101]. The reduction of the quantity of microcolonies adhered on the bone surface was directly related to the CO contained in AG coating of the surface of nanoparticles, since this antibiotic has a destabilising effect on *E. coli* biofilm matrix structure and it can lead to the release of planktonic cells, which are more susceptible to antibiotics [77]. Hence, the use of AG+CO-coated MX-loaded MSNs showed a cooperative effect between both antibiotics, confirming the suitability of using this nanocarrier for the treatment of bone infections caused by *E. coli*.

Bone infections are linked with progressive inflammatory tissue destruction and can induce marked local bone resorption at sites of infection and proximal abnormal bone formation. Overall, three types of cells are responsible for this process, namely osteoblasts/osteocytes, osteoclasts and macrophages, although others can be involved [102]. Nevertheless, the lowest cytotoxicity median value was ranged between 93.5% for 31.25 μg/mL and 94.54% for 62.5 μg/mL, which can be considered as low for all types of cells used according to previously published studies [103]. The reduction of cell proliferation would be a consequence of two antibiotics used, CO and MX, as observed in both osteoblasts (at 14 days) and macrophages. CO can inhibit cell proliferation in a dose-dependent and time-dependent manner [104], whilst MX has shown an an-

tiproliferative effect on certain cells [105], as reported previously by other authors that used moxifloxacin as cargo in sol-gel-based materials [106]. In this sense, the use of nanoparticles to deliver these antibiotics would imply the administration of lower doses and the decrease of their side effects [107–110]. Hence, our treatment would entail a transient antiproliferative effect for the sake of an effective anti-bacterial benefit in the treatment of bone infections. It is noteworthy that osteoblasts exposed to the higher dose (62.5 μg/mL) showed superior proliferation at 21 days than those exposed to the lower dose (31.25 μg/mL). We hypothesize that this behavior might stem from the Arabic gum coating of the MSNs, which might favour the osteoblastic proliferation in the long term. This would be in agreement with the finding that gum tragacanth can promote the adhesion, proliferation, and osteogenic differentiation of adipose-derived mesenchymal stem cells [111].

MSNs tend to accumulate in the reticuloendothelial system, which consists of cells descending from the monocytes able to perform phagocytosis of foreign materials [112]. Up to 90% of the reticuloendothelial system is located in the liver [113]. Hepatic reticuloendothelial system includes endothelial cells, Kupffer cells (KCs), fat storing cells and pit cells [114]. KCs have special surface structures responsible for the phagocytotic capacity, the so-called fuzzy coat [114]. This phagocytic activity can cause their activation and the production of a number of cell signaling and stress pathway modulators, e.g. reactive oxygen species and cytokines such as TNF-α [57]. This factor promotes the synthesis of IL-6 both in KC and in endothelial cells and in liver stelae, which is a cytokine involved in the proliferation of hepatocyte cells [115]. CYP3A is an enzyme mainly found in the liver and in the intestine able to oxidize small foreign organic molecules, such as toxins or drugs [116]. Due to the role of the liver on systemic administration of MSNs, we decided to evaluate the hepatotoxicity of our nanosystem on a hepatocyte-KCs co-culture model. As shown in Fig. 10, AG+CO-coated MX-loaded MSNs provoked a statistically significant increase of TNF-α concentration and a significant decrease of IL-6 concentration. An increase in TNF-α precedes the onset of hepatic parenchymal cell injury [117], that, in this scenario, could be reflected on the reduced IL-6 production by KCs and hepatic CYP3A activity. Even though there are up to three Kupffer cell-mediated clearance pathways of MSNs (endocytosis, phagocytosis, and micropinocytosis) [118], AG+CO-coated MX-loaded MSNs uptake by KCs was not observed in hepatocyte-KCs co-culture (data not shown). Thus, the hepatoxicity associated to AG+CO-coated MX-loaded MSNs observed in our results might be due to the effect of the high amount of colistin loaded by AG+CO coating, hepatotoxicity that has already been described in a patient with Gram-negative rod bacteremia treated intramuscularly with colistin [119]. This hypothesis derived from the *in vitro* hepatic model would be further supported by the pathological findings on the livers of the rabbits that received a single intravenous dose of nanoparticles, which showed mild signs of ductulitis with signs of lymphocytosis in bile ducts (Fig. 11). This would point out that these nanoparticles could cross the endothelium into the Disse space, from where they could be slowly returned to lymphatic circulation, taken up by hepatocytes or subsequently involved in a biliary excretion pathway [118]. This transient passage through the liver parenchyma would be favoured by the size of AG+CO-coated MX-loaded MSNs (~190 nm), which is within the range of the fenestration diameter (100–200 nm) of the endothelium of hepatic sinusoid [120], and would be slow enough to result in local lymphocytosis around the bile ducts. This finding would vouch the use of local (specifically intraosseous), rather than systemic, administration of nanoparticles. The rationale behind this benefit can be explained as follows. Rapid bloodstream clearance of nanoparticles after intravenous administration has long been recognized as a major barrier to drug delivery [121]. In this sense, it has been recently discovered that administering a dose that surpasses the maximum Kupffer cell uptake rate significantly diminishes the proportion of nanoparticles taken up by the reticuloendothelial system [122]. In consequence, maintaining a significant dose in the blood would imply the need to administer a rather large dose of nanoparticles, which would inherently yield higher hepatic damage. Conversely, injecting the nanoparticles in a localized manner allows to achieve high drug concentration right at the infection site by using a significantly lower quantity of nanoparticles. Hence, this approach would diminish the potential organ damage owing to the lower dose injected.

As observed in Fig. 12, AG+CO-coated MX-loaded MSNs treatment was able to eradicate completely the osteomyelitis provoked by *E. coli* in two out of three rabbit and to reduce the bacterial concentration more than 99% in the remaining animal. The pathological findings also supported the microbiological results. The livers of control group showed a mild-moderate central perivenous portal inflammation and minimal lobular hepatitis accompanied by an inflammatory infiltrate consisting of lymphocytes, plasma cells and eosinophils, a suggestive indicator of an infectious process in the rabbits [123]; the liver of treated rabbits just showed the same histological signs derived from the intraosseous administration of AG+CO-coated MX-loaded MSNs that will inevitably end up reaching the systemic circulation and being taken up by the liver, except that it will do so later and in lower concentration than if administered intravenously.

In light of our results, AG+CO-coated MX-loaded MSNs arise as a novel strategy for the localized treatment of bone infections, involving minimal recruitment of the reticuloendothelial organs (e.g. liver and kidneys). Indeed, this nanoformulation could be incorporated or combined with existing ones, including, antibiotic-loaded collagen sponges [124], bone cements [125], or new treatment approaches, e.g. hydrogels [126,127], polymers [128], or microplates [129].

This study is not exempt from limitations. First, despite Gram-negative bacteria suppose an increasing threat to bone-associated infections, they still represent a reduced percentage of all these infections. In this regard, the rationale behind our therapeutic approach could be employed for the development of a similar nanosystem specifically designed for the treatment of Gram-positive infection related to bone. Second, *E. coli* stands out among the Gram-negative bacteria for their ability to develop antibiotic resistance. For that reason, we considered it a reasonable bacterial model to test our nanosystem, although more additional Gram-negative bacteria relevant to osteomyelitis, e.g., *Pseudomonas aeruginosa*, should be further evaluated. Furthermore, moxifloxacin has been employed here as an example antibiotic loadable in MSNs. However, because quinolone resistance is increasing worldwide [130], these nanoparticles might be specifically loaded with alternative fluoroquinolones or other antibiotics according to the geographic prevalence of antibiotic resistance to ensure good infection outcome.

5. Conclusion

In this work, moxifloxacin-loaded mesoporous silica nanoparticles have been successfully functionalized with Arabic gum plus colistin (AG+CO-coated MX-loaded MSNs) to be employed in the treatment of bone infections cause by *E. coli*. The nanosystem demonstrated high affinity toward *E. coli* biofilm matrix, thanks to AG coating, and marked antibacterial effect because of the bactericidal effect of moxifloxacin and the disaggregating effect of colistin. AG+CO-coated MX-loaded MSNs were able to eradicate the infection developed on a trabecular bone *in vitro* and showed pronounced antibacterial efficacy *in vivo* against an osteomyelitis provoked by *E. coli*. Furthermore, AG+CO-coated MX-loaded MSNs

were shown to be essentially non-cytotoxic with only slight effect on cell proliferation and mild hepatotoxicity, which might be attributed to the nature of both antibiotics. In view of these results, these nanoparticles may be considered as a promising treatment for bone infections caused by enterobacteria, such as *E. coli*, and introduce a general strategy against bone infections based on the implementation of antibiotics with different but complementary activity into a single nanocarrier.

Declaration of Competing Interest

The authors declare that they have no known competing financial interests or personal relationships that could have appeared to influence the work reported in this paper.

CRediT authorship contribution statement

J.J. Aguilera-Correa: Conceptualization, Methodology, Software, Validation, Formal analysis, Investigation, Data curation, Writing – original draft, Writing – review & editing, Visualization. **M. Gisbert-Garzarán:** Validation, Formal analysis, Investigation, Data curation, Writing – original draft, Writing – review & editing, Visualization. **A. Mediero:** Investigation, Writing – original draft, Writing – review & editing, Visualization. **R.A. Carias-Cálix:** Investigation, Writing – original draft, Visualization. **C. Jiménez-Jiménez:** Investigation, Writing – original draft, Visualization. **J. Esteban:** Validation, Writing – review & editing, Visualization. **M. Vallet-Regí:** Validation, Resources, Writing – review & editing, Visualization, Project administration, Funding acquisition.

Acknowledgments

The authors acknowledge the financial support from the European Research Council through ERC-2015-AdG-694160 (VERDI) grant. AM is funded by grants from Instituto de Salud Carlos III through the "Miguel Servet" program (CP15/00053). We also wish to acknowledge María del Mar González García-Parreño for her help with the use of the confocal laser-scanning microscope and Dr Ana Conde, Dr Marían ángeles Arenas-Vara and Dr. Juan José de Damborenea from National Center for Metallurgical Research (CENIM-CSIC) for manufacturing the Ti-6Al-4V implants used in the *in vivo* model of this study. Parts of this work were previously presented at the 31st European Congress of Clinical Microbiology and Infectious Diseases, and 24th Spanish Congress of Clinical Microbiology and Infectious Diseases. Graphical abstract, Scheme 1, Fig. S4, and some icons from Figs. 11 and 13 have been created with BioRender.com.

Supplementary materials

Supplementary material associated with this article can be found, in the online version, at doi:10.1016/j.actbio.2021.10.014.

References

[1] M.C. Birt, D.W. Anderson, E. Bruce Toby, J. Wang, Osteomyelitis: recent advances in pathophysiology and therapeutic strategies, J. Orthop. 14 (2017) 45–52, doi:10.1016/j.jor.2016.10.004.
[2] H.M. Kremers, M.E. Nwojo, J.E. Ransom, C.M. Wood-Wentz, L.J. Melton, P.M. Huddleston, Trends in the epidemiology of osteomyelitis: a population-based study, 1969 to 2009, J. Bone Joint Surg. Am. 97 (2015) 837–845, doi:10.2106/JBJS.N.01350.
[3] F. Lobati, B. Herndon, D. Bamberger, Osteomyelitis: etiology, diagnosis, treatment and outcome in a public versus a private institution, Infection 29 (2001) 333–336, doi:10.1007/s15010-001-1134-6.
[4] N. Benito, M. Franco, A. Ribera, A. Soriano, D. Rodriguez-Pardo, L. Sorlí, G. Fresco, M. Fernández-Sampedro, M. Dolores del Toro, L. Guío, E. Sánchez-Rivas, A. Bahamonde, M. Riera, J. Esteban, J.M. Baraia-Etxaburu, J. Martínez-Alvarez, A. Jover-Sáenz, C. Dueñas, A. Ramos, B. Sobrino, G. Euba, L. Morata, C. Pigrau, P. Coll, I. Mur, J. Ariza, F. Barcenilla, F. Pérez-Villar, L. Prats-Gispert, R. Cisterna, S. Ibarra, Í. López, J.M. Santamaría, J. Cabo, D. García, J. Lora-Tamayo, O. Murillo, S. Pedrero, S. Álvarez-Parrondo, R. Muedra-Font, C. Raya-Fernández, C. Rodríguez-Alonso, A. Moreno, M.A. Blanco-Martínez-de-Morentin, R. Cabo-Magadan, A. Combalia, S. García, J.C. Martínez-Pastor, E. Tornero, J. Merino-Pérez, J.M. Montejo, A. Alier, J.P. Horcajada, V. Plasencia, L. Puig, Á. Auñon, A. Blanco, J. García-Cañete, E. Sandoval, M. Fakkas-Fernández, C. Garcés-Zarzalejo, C. Fariñas-Alvarez, M.C. Fariñas, L. Martinez-Martinez, C. Salas-Venero, J. Cobo, P. Ruiz-Carbajosa, M. Jordán, X. Crusi, C. Marinescu, F. Montaner, A. Ramírez, P.S. Corona, M. Lung, M.Á. Muniain-Ezcurra, C. Peñas-Espinar, A.I. Suárez, R. Álvarez, J.-A. Cordero, M. López-Pliego, J. Palomino, A. Puente, Time trends in the aetiology of prosthetic joint infections: a multicentre cohort study, Clin. Microbiol. Infect. 22 (2016) 732.e1-732.e8, doi:10.1016/j.cmi.2016.05.004.
[5] N. Benito, I. Mur, A. Ribera, A. Soriano, D. Rodríguez-Pardo, L. Sorlí, J. Cobo, M. Fernández-Sampedro, M. del Toro, L. Guío, J. Praena, A. Bahamonde, M. Riera, J. Esteban, J. Baraia-Etxaburu, J. Martínez-Alvarez, A. Jover-Sáenz, C. Dueñas, A. Ramos, B. Sobrino, G. Euba, L. Morata, C. Pigrau, J. Horcajada, P. Coll, X. Crusi, J. Ariza, On behalf of the REIPI (Spanish Network for Research in Infectious Disease) Group for the Study of Prosthetic Joint Infections/GEIO (Group for the Study of Osteoarticular Infections), SEIMC (Spanish Society of Infectious Diseases and Clinical Microbiolo, The different microbial etiology of prosthetic joint infections according to route of acquisition and time after prosthesis implantation, including the role of multidrug-resistant organisms, JCM 8 (2019) 673, doi:10.3390/jcm8050673.
[6] J.D.D. Pitout, Multiresistant enterobacteriaceae: new threat of an old problem, Expert Rev. Anti. Infect. Ther. 6 (2008) 657–669, doi:10.1586/14787210.6.5.657.
[7] M. Delgado-Valverde, J. Sojo-Dorado, A. Pascual, J. Rodríguez-Baño, Clinical management of infections caused by multidrug-resistant Enterobacteriaceae, Ther. Adv. Infect. Dis. 1 (2013) 49–69, doi:10.1177/2049936113476284.
[8] E.A. Masters, R.P. Trombetta, K.L. de Mesy Bentley, B.F. Boyce, A.L. Gill, S.R. Gill, K. Nishitani, M. Ishikawa, Y. Morita, H. Ito, S.N. Bello-Irizarry, M. Ninomiya, J.D. Brodell, C.C. Lee, S.P. Hao, I. Oh, C. Xie, H.A. Awad, J.L. Daiss, J.R. Owen, S.L. Kates, E.M. Schwarz, G. Muthukrishnan, Evolving concepts in bone infection: redefining "biofilm", "acute vs. chronic osteomyelitis", "the immune proteome" and "local antibiotic therapy, Bone Res. 7 (2019) 20, doi:10.1038/s41413-019-0061-z.
[9] J.M. Fritz, J.R. McDonald, Osteomyelitis: approach to diagnosis and treatment, Phys. Sportsmed. 36 (2008) nihpa116823, doi:10.3810/psm.2008.12.11.
[10] R.C. Fang, R.D. Galiano, Adjunctive therapies in the treatment of osteomyelitis, Semin. Plast. Surg. 23 (2009) 141–147, doi:10.1055/s-0029-1214166.
[11] H. Ragelle, F. Danhier, V. Préat, R. Langer, D.G. Anderson, Nanoparticle-based drug delivery systems: a commercial and regulatory outlook as the field matures, Expert Opin. Drug Deliv. 14 (2017) 851–864, doi:10.1080/17425247.2016.1244187.
[12] M. Vallet-Regi, A. Rámila, R.P. del Real, J. Pérez-Pariente, A new property of MCM-41: drug delivery system, Chem. Mater. 13 (2001) 308–311, doi:10.1021/cm0011559.
[13] M. Manzano, M. Vallet-Regí, Mesoporous silica nanoparticles for drug delivery, Adv. Funct. Mater. 30 (2020) 1902634, doi:10.1002/adfm.201902634.
[14] J. Lu, M. Liong, Z. Li, J.I. Zink, F. Tamanoi, Biocompatibility, biodistribution, and drug-delivery efficiency of mesoporous silica nanoparticles for cancer therapy in animals, Small 6 (2010) 1794–1805, doi:10.1002/smll.201000538.
[15] J.L. Vivero-Escoto, I.I. Slowing, B.G. Trewyn, V.S.Y. Lin, Mesoporous silica nanoparticles for intracellular controlled drug delivery, Small 6 (2010) 1952–1967, doi:10.1002/smll.200901789.
[16] M. Gisbert-Garzarán, M. Manzano, M. Vallet-Regí, Mesoporous silica nanoparticles for the treatment of complex bone diseases: bone cancer, bone infection and osteoporosis, Pharmaceutics 12 (2020) 83, doi:10.3390/pharmaceutics12010083.
[17] L. Polo, N. Gómez-Cerezo, E. Aznar, J.L. Vivancos, F. Sancenón, D. Arcos, M. Vallet-Regí, R. Martínez-Máñez, Molecular gates in mesoporous bioactive glasses for the treatment of bone tumors and infection, Acta Biomater. 50 (2017) 114–126, doi:10.1016/j.actbio.2016.12.025.
[18] L. Polo, N. Gómez-Cerezo, A. García-Fernández, E. Aznar, J.L. Vivancos, D. Arcos, M. Vallet-Regí, R. Martínez-Máñez, Mesoporous bioactive glasses equipped with stimuli-responsive molecular gates for controlled delivery of levofloxacin against bacteria, Chem. Eur. J. 24 (2018) 18944–18951, doi:10.1002/chem.201803301.
[19] A. Aguilar-Colomer, M. Colilla, I. Izquierdo-Barba, C. Jiménez-Jiménez, I. Mahillo, J. Esteban, M. Vallet-Regí, Impact of the antibiotic-cargo from MSNs on gram-positive and gram-negative bacterial biofilms, Microporous Mesoporous Mater. 311 (2021) 110681, doi:10.1016/j.micromeso.2020.110681.
[20] M. Colilla, M. Vallet-Regí, Targeted Stimuli-responsive mesoporous silica nanoparticles for bacterial infection treatment, IJMS 21 (2020) 8605, doi:10.3390/ijms21228605.
[21] J.A. Barman Balfour, L.R. Wiseman, Moxifloxacin, Drugs 57 (1999) 363–373, doi:10.2165/00003495-199957030-00007.
[22] R. San Juan, A. Garcia-Reyne, P. Caba, F. Chaves, C. Resines, F. Llanos, F. López-Medrano, M. Lizasoain, J.M. Aguado, Safety and efficacy of moxifloxacin monotherapy for treatment of orthopedic implant-related staphylococcal infections, Antimicrob. Agents Chemother. 54 (2010) 5161–5166, doi:10.1128/AAC.00027-10.
[23] L. Malincarne, M. Ghebregzabher, M.V. Moretti, A.M. Egidi, B. Canovari, G. Tavolieri, D. Francisci, G. Cerulli, F. Baldelli, Penetration of moxifloxacin into

bone in patients undergoing total knee arthroplasty, J.Antimicrob. Chemother. 57 (2006) 950–954, doi:10.1093/jac/dkl091.
[24] V. Soranoglou, I. Galanopoulos, E.J. Giamarellos-Bourboulis, A. Papalois, E. Giannitsioti, L.A. Poultsides, T. Choreftaki, K. Kanellakopoulou, Efficacy of intramuscular moxifloxacin in the treatment of experimental osteomyelitis caused by methicillin-resistant Staphylococcus aureus, Int. J. Antimicrob. Agents 50 (2017) 186–190, doi:10.1016/j.ijantimicag.2017.01.041.
[25] R.L. Nation, J. Li, Colistin in the 21st century, Curr. Opin. Infect. Dis. 22 (2009) 535–543, doi:10.1097/QCO.0b013e328332e672.
[26] S. Corvec, U. Furustrand Tafin, B. Betrisey, O. Borens, A. Trampuz, Activities of fosfomycin, tigecycline, colistin, and gentamicin against extended-spectrum-β-lactamase-producing Escherichia coli in a foreign-body infection model, Antimicrob. Agents Chemother. 57 (2013) 1421–1427, doi:10.1128/AAC.01718-12.
[27] B.H. Ali, A. Ziada, G. Blunden, Biological effects of gum arabic: a review of some recent research, Food Chem. Toxicol. 47 (2009) 1–8, doi:10.1016/j.fct.2008.07.001.
[28] M. Gisbert-Garzaran, D. Lozano, M. Vallet-Regí, M. Manzano, Self-immolative polymers as novel pH-responsive gate keepers for drug delivery, RSC Adv. 7 (2017) 132–136, doi:10.1039/C6RA26771H.
[29] M. Maqbool, A. Ali, P.G. Alderson, M.T.M. Mohamed, Y. Siddiqui, N. Zahid, Postharvest application of gum arabic and essential oils for controlling anthracnose and quality of banana and papaya during cold storage, Postharvest Biol. Technol. 62 (2011) 71–76, doi:10.1016/j.postharvbio.2011.04.002.
[30] U. Lendenmann, M. Snozzi, T. Egli, Growth kinetics of *Escherichia coli* with galactose and several other sugars in carbon-limited chemostat culture, Can. J. Microbiol. 46 (2000) 72–80, doi:10.1139/cjm-46-1-72.
[31] S.H. Baien, J. Seele, T. Henneck, C. Freibrodt, G. Szura, H. Moubasher, R. Nau, G. Brogden, M. Morgelin, M. Singh, M. Kietzmann, M. von Köckritz-Blickwede, N. de Buhr, Antimicrobial and immunomodulatory effect of gum arabic on human and bovine granulocytes against staphylococcus aureus and Escherichia coli, Front. Immunol. 10 (2020) 3119, doi:10.3389/fimmu.2019.03119.
[32] Z. Gounani, M.A. Asadollahi, Jannik.N. Pedersen, J. Lyngsø, J. Skov Pedersen, A. Arpanaei, R.L. Meyer, Mesoporous silica nanoparticles carrying multiple antibiotics provide enhanced synergistic effect and improved biocompatibility, Colloids Surf. B Biointerfaces 175 (2019) 498–508, doi:10.1016/j.colsurfb.2018.12.035.
[33] Thomas Subramaniam, Jambhrunkar Gustafsson, Prestidge Kidd, Rifampicin-loaded mesoporous silica nanoparticles for the treatment of intracellular infections, Antibiotics 8 (2019) 39, doi:10.3390/antibiotics8020039.
[34] Á. Auñón, J. Esteban, A.L. Doadrio, M. Boiza-Sánchez, A. Mediero, D. Eguibar-Blázquez, J. Cordero-Ampuero, A. Conde, M. Arenas, J. de-Damborenea, J.J. Aguilera-Correa, *Staphylococcus aureus* prosthetic joint infection is prevented by a fluorine- and phosphorus-doped nanostructured Ti–6Al–4V alloy loaded with gentamicin and vancomycin, J. Orthop. Res. 38 (2020) 588–597, doi:10.1002/jor.24496.
[35] A.L. Doadrio, A. Conde, M.A. Arenas, J.M. Hernández-López, J.J. de Damborenea, C. Pérez-Jorge, J. Esteban, M. Vallet-Regí, Use of anodized titanium alloy as drug carrier: Ibuprofen as model of drug releasing, Int. J. Pharm. 492 (2015) 207–212, doi:10.1016/j.ijpharm.2015.07.046.
[36] J.J. Aguilera-Correa, A.L. Doadrio, A. Conde, M.A. Arenas, J.J. de-Damborenea, M. Vallet-Regí, J. Esteban, Antibiotic release from *F*-doped nanotubular oxide layer on TI6AL4V alloy to decrease bacterial viability, J. Mater. Sci. Mater. Med. 29 (2018) 118, doi:10.1007/s10856-018-6119-4.
[37] S.S. Aiken, J.J. Cooper, H. Florance, M.T. Robinson, S. Michell, Local release of antibiotics for surgical site infection management using high-purity calcium sulfate: an *in vitro* elution study, Surg. Infect. 16 (2015) 54–61 (Larchmt), doi:10.1089/sur.2013.162.
[38] L.É. Uhljar, S.Y. Kan, N. Radacsi, V. Koutsos, P. Szabó-Révész, R. Ambrus, *In vitro* drug release, permeability, and structural test of ciprofloxacin-loaded nanofibers, Pharmaceutics 13 (2021) 556, doi:10.3390/pharmaceutics13040556.
[39] J.A. Ocaña, F.J. Barragán, M. Callejón, Spectrofluorimetric determination of moxifloxacin in tablets, human urine and serum, Analyst 125 (2000) 2322–2325, doi:10.1039/b005991i.
[40] S. DeLeon, A. Clinton, H. Fowler, J. Everett, A.R. Horswill, K.P. Rumbaugh, Synergistic interactions of pseudomonas aeruginosa and staphylococcus aureus in an *in vitro* wound model, Infect. Immun. 82 (2014) 4718–4728, doi:10.1128/IAI.02198-14.
[41] Y. Sun, S.E. Dowd, E. Smith, D.D. Rhoads, R.D. Wolcott, *In vitro* multispecies Lubbock chronic wound biofilm model, Wound Repair Regen. 16 (2008) 805–813, doi:10.1111/j.1524-475X.2008.00434.x.
[42] S. Stepanović, D. Vuković, V. Hola, G. Di Bonaventura, S. Djukić, I. Cirković, F. Ruzicka, Quantification of biofilm in microtiter plates: overview of testing conditions and practical recommendations for assessment of biofilm production by staphylococci, APMIS 115 (2007) 891–899, doi:10.1111/j.1600-0463.2007.apm_630.x.
[43] R.K. Pettit, C.A. Weber, G.R. Pettit, Application of a high throughput Alamar blue biofilm susceptibility assay to Staphylococcus aureus biofilms, Ann. Clin. Microbiol. Antimicrob. 8 (2009) 28, doi:10.1186/1476-0711-8-28.
[44] E. Limpens, S. Ivanov, W. van Esse, G. Voets, E. Fedorova, T. Bisseling, *Medicago* N_2 -fixing symbiosomes acquire the endocytic identity marker rab7 but delay the acquisition of vacuolar identity, Plant Cell 21 (2009) 2811–2828, doi:10.1105/tpc.108.064410.
[45] CLSI. Methods for dilution antimicrobial susceptibility tests for bacteria that grow aerobically. 11th ed. CLSI standard M07. Wayne, PA: Clinical and Laboratory Standards Institute; 2018.
[46] C. Hernandes, J. da S. Coppede, B.W. Bertoni, S. de C. França, A.M.S. Pereira, *Flash microbiocide*: a rapid and economic method for determination of MBC and MFC, AJPS 04 (2013) 850–852, doi:10.4236/ajps.2013.44104.
[47] H. Ceri, M.E. Olson, C. Stremick, R.R. Read, D. Morck, A. Buret, The calgary biofilm device: new technology for rapid determination of antibiotic susceptibilities of bacterial biofilms, J. Clin. Microbiol. 37 (1999) 1771–1776, doi:10.1128/JCM.37.6.1771-1776.1999.
[48] Y. Sun, S.E. Dowd, E. Smith, D.D. Rhoads, R.D. Wolcott, *In vitro* multispecies Lubbock chronic wound biofilm model: chronic wound biofilm model, Wound Repair Regen. 16 (2008) 805–813, doi:10.1111/j.1524-475X.2008.00434.x.
[49] E. Peeters, H.J. Nelis, T. Coenye, *In vitro* activity of ceftazidime, ciprofloxacin, meropenem, minocycline, tobramycin and trimethoprim/sulfamethoxazole against planktonic and sessile Burkholderia cepacia complex bacteria, J. Antimicrob. Chemother. 64 (2009) 801–809, doi:10.1093/jac/dkp253.
[50] J. Esteban, E. Gomez-Barrena, J. Cordero, N.Z. Martín-de-Hijas, T.J. Kinnari, R. Fernandez-Roblas, Evaluation of quantitative analysis of cultures from sonicated retrieved orthopedic implants in diagnosis of orthopedic infection, J. Clin. Microbiol. 46 (2008) 488–492, doi:10.1128/JCM.01762-07.
[51] B. Herigstad, M. Hamilton, J. Heersink, How to optimize the drop plate method for enumerating bacteria, J. Microbiol. Methods 44 (2001) 121–129, doi:10.1016/s0167-7012(00)00241-4.
[52] G.J. Oostingh, E. Casals, P. Italiani, R. Colognato, R. Stritzinger, J. Ponti, T. Pfaller, Y. Kohl, D. Ooms, F. Favilli, H. Leppens, D. Lucchesi, F. Rossi, I. Nelissen, H. Thielecke, V.F. Puntes, A. Duschl, D. Boraschi, Problems and challenges in the development and validation of human cell-based assays to determine nanoparticle-induced immunomodulatory effects, Part Fibre Toxicol. 8 (2011) 8, doi:10.1186/1743-8977-8-8.
[53] S.S. Hakki, B.S. Bozkurt, E.E. Hakki, Boron regulates mineralized tissue-associated proteins in osteoblasts (MC3T3-E1), J.Trace Elem. Med. Biol. 24 (2010) 243–250, doi:10.1016/j.jtemb.2010.03.003.
[54] X. Yuan, H. Cao, J. Wang, K. Tang, B. Li, Y. Zhao, M. Cheng, H. Qin, X. Liu, X. Zhang, Immunomodulatory effects of calcium and strontium co-doped titanium oxides on Osteogenesis, Front. Immunol. 8 (2017) 1196, doi:10.3389/fimmu.2017.01196.
[55] A.Y. Ng, C. Tu, S. Shen, D. Xu, M.J. Oursler, J. Qu, S. Yang, Comparative characterization of osteoclasts derived from murine bone marrow macrophages and RAW 264.7 cells using quantitative proteomics: proteomic comparison of osteoclast modelS, JBMR Plus 2 (2018) 328–340, doi:10.1002/jbm4.10058.
[56] E.L. LeCluyse, P.L. Bullock, A. Parkinson, J.H. Hochman, Cultured Rat Hepatocytes, in: R.T. Borchardt, P.L. Smith, G. Wilson (Eds.), Models for Assessing Drug Absorption and Metabolism, Springer US, Boston, MA, 1996, pp. 121–159, doi:10.1007/978-1-4899-1863-5_9.
[57] K.A. Rose, N.S. Holman, A.M. Green, M.E. Andersen, E.L. LeCluyse, Co-culture of hepatocytes and Kupffer cells as an *in vitro* model of inflammation and drug-induced hepatotoxicity, J. Pharm. Sci. 105 (2016) 950–964, doi:10.1016/S0022-3549(15)00192-6.
[58] P.M. Baby, P. Kumar, R. Kumar, S.S. Jacob, D. Rawat, V.S. Binu, K.M. Karun, A novel method for blood volume estimation using trivalent chromium in rabbit models, Indian J. Plast. Surg. 47 (2014) 242–248, doi:10.4103/0970-0358.138961.
[59] F. Faul, E. Erdfelder, A.G. Lang, A. Buchner, G*Power 3: a flexible statistical power analysis program for the social, behavioral, and biomedical sciences, Behav. Res. Methods 39 (2007) 175–191, doi:10.3758/bf03193146.
[60] J.J. Aguilera-Correa, Á. Auñón, M. Boiza-Sánchez, I. Mahillo-Fernández, A. Mediero, D. Eguibar-Blázquez, A. Conde, M.Á. Arenas, J.J. de-Damborenea, J. Cordero-Ampuero, J. Esteban, Urine aluminum concentration as a possible implant biomarker of *pseudomonas aeruginosa* infection using a fluorine- and phosphorus-doped Ti-6Al-4V alloy with osseointegration capacity, ACS Omega 4 (2019) 11815–11823, doi:10.1021/acsomega.9b00898.
[61] Á. Auñón, J. Esteban, A.L. Doadrio, M. Boiza-Sánchez, A. Mediero, D. Eguibar-Blázquez, J. Cordero-Ampuero, A. Conde, M. Arenas, J. de-Damborenea, J.J. Aguilera-Correa, *Staphylococcus aureus* prosthetic joint infection is prevented by a fluorine- and phosphorus-doped nanostructured Ti–6Al–4V alloy loaded with gentamicin and vancomycin, J. Orthop. Res. 38 (2020) 588–597, doi:10.1002/jor.24496.
[62] J.L. Paris, M.V. Cabañas, M. Manzano, M. Vallet-Regí, Polymer-grafted mesoporous silica nanoparticles as ultrasound-responsive drug carriers, ACS Nano 9 (2015) 11023–11033, doi:10.1021/acsnano.5b04378.
[63] F. Balas, M. Manzano, M. Colilla, M. Vallet-Regí, L-Trp adsorption into silica mesoporous materials to promote bone formation, Acta Biomater. 4 (2008) 514–522, doi:10.1016/j.actbio.2007.11.009.
[64] T. Bjarnsholt, M. Alhede, M. Alhede, S.R. Eickhardt-Sørensen, C. Moser, M. Kühl, P.Ø. Jensen, N. Høiby, The *in vivo* biofilm, Trends Microbiol. 21 (2013) 466–474, doi:10.1016/j.tim.2013.06.002.
[65] B.Y. Lee, Z. Li, D.L. Clemens, B.J. Dillon, A.A. Hwang, J.I. Zink, M.A. Horwitz, Redox-triggered release of moxifloxacin from mesoporous silica nanoparticles functionalized with disulfide snap-tops enhances efficacy against pneumonic tularemia in mice, Small 12 (2016) 3690–3702, doi:10.1002/smll.201600892.
[66] Z. Li, D.L. Clemens, B.Y. Lee, B.J. Dillon, M.A. Horwitz, J.I. Zink, Mesoporous silica nanoparticles with pH-sensitive nanovalves for delivery of moxifloxacin provide improved treatment of lethal pneumonic tularemia, ACS Nano 9 (2015) 10778–10789, doi:10.1021/acsnano.5b04306.

[67] I. Otri, S. El Sayed, S. Medaglia, R. Martínez-Máñez, E. Aznar, F. Sancenón, Simple endotoxin detection using polymyxin-B-gated nanoparticles, Chem. Eur. J. 25 (2019) 3770–3774, doi:10.1002/chem.201806306.

[68] Z. Gounani, M.A. Asadollahi, R.L. Meyer, A. Arpanaei, Loading of polymyxin B onto anionic mesoporous silica nanoparticles retains antibacterial activity and enhances biocompatibility, Int. J. Pharm. 537 (2018) 148–161, doi:10.1016/j.ijpharm.2017.12.039.

[69] M. Martínez-Carmona, Y.K. Gun'ko, M. Vallet-Regí, Mesoporous silica materials as drug delivery: "The Nightmare" of bacterial infection, Pharmaceutics 10 (2018), doi:10.3390/pharmaceutics10040279.

[70] H. Younes, N. Egret, M. Hadj-Abdelkader, C. Rémésy, C. Demigné, C. Gueret, P. Deteix, J.C. Alphonse, Fermentable carbohydrate supplementation alters nitrogen excretion in chronic renal failure, J. Ren. Nutr. 16 (2006) 67–74, doi:10.1053/j.jrn.2005.10.007.

[71] A. Kishimoto, K. Ushida, G.O. Phillips, T. Ogasawara, Y. Sasaki, Identification of intestinal bacteria responsible for fermentation of gum arabic in pig model, Curr. Microbiol. 53 (2006) 173–177, doi:10.1007/s00284-005-0219-3.

[72] H. Ahallil, A. Abdullah, M.Y. Maskat, S.R. Sarbini, Fermentation of Gum Arabic by Gut Microbiota Using *In Vitro* Colon Model, Selangor, Malaysia, 2019, doi:10.1063/1.5111252.

[73] H.A. Heydary, E. Karamian, E. Poorazizi, A. Khandan, J. Heydaripour, A novel nano-fiber of iranian gum tragacanth-polyvinyl alcohol/nanoclay composite for wound healing applications, Procedia Mate. Sci. 11 (2015) 176–182, doi:10.1016/j.mspro.2015.11.079.

[74] J. Wingender, K.E. Jaeger, Extracellular enzymes in Biofilms, in: G. Bitton (Ed.), Encyclopedia of Environmental Microbiology, John Wiley & Sons, Inc., Hoboken, NJ, USA, 2003, p. env261, doi:10.1002/0471263397.env261.

[75] X. Huang, M. Li, Y. Xu, J. Zhang, X. Meng, X. An, L. Sun, L. Guo, X. Shan, J. Ge, J. Chen, Y. Luo, H. Wu, Y. Zhang, Q. Jiang, X. Ning, Novel gold nanorod-based HR1 peptide inhibitor for middle east respiratory syndrome coronavirus, ACS Appl. Mater. Interfaces 11 (2019) 19799–19807, doi:10.1021/acsami.9b04240.

[76] S.P. Lapage, M.S. Jayaraman, Beta-galactosidase and lactose fermentation in the identification of enterobacteria including salmonellae, J. Clin. Pathol. 17 (1964) 117–121, doi:10.1136/jcp.17.2.117.

[77] M. Klinger-Strobel, C. Stein, C. Forstner, O. Makarewicz, M.W. Pletz, Effects of colistin on biofilm matrices of Escherichia coli and Staphylococcus aureus, Int. J. Antimicrob. Agents 49 (2017) 472–479, doi:10.1016/j.ijantimicag.2017.01.005.

[78] G. Dodi, A. Pala, E. Barbu, D. Peptanariu, D. Hritcu, M.I. Popa, B.I. Tamba, Carboxymethyl guar gum nanoparticles for drug delivery applications: preparation and preliminary *in-vitro* investigations, Mater. Sci. Eng. C Mater. Biol. Appl. 63 (2016) 628–636, doi:10.1016/j.msec.2016.03.032.

[79] M. Kaur, B. Malik, T. Garg, G. Rath, A.K. Goyal, Development and characterization of guar gum nanoparticles for oral immunization against tuberculosis, Drug Deliv. 22 (2015) 328–334, doi:10.3109/10717544.2014.894594.

[80] M. Sharma, R. Malik, A. Verma, P. Dwivedi, G.S. Banoth, N. Pandey, J. Sarkar, P.R. Mishra, A.K. Dwivedi, Folic acid conjugated guar gum nanoparticles for targeting methotrexate to colon cancer, J. Biomed. Nanotechnol. 9 (2013) 96–106, doi:10.1166/jbn.2013.1474.

[81] J.K. Sarmah, R. Mahanta, S.K. Bhattacharjee, R. Mahanta, A. Biswas, Controlled release of tamoxifen citrate encapsulated in cross-linked guar gum nanoparticles, Int. J. Biol. Macromol. 49 (2011) 390–396, doi:10.1016/j.ijbiomac.2011.05.020.

[82] M. Razavi, Hydrogels: types, structure, properties, and applications, in: Frontiers in Biomaterials, 4, Bentham Science Publishers Ltd., UAE, 2017, pp. 143–169, doi:10.2174/9781681085364117040007.

[83] M.A. Maghsoudlou, E. Nassireslami, S. Saber-Samandari, A. Khandan, Bone regeneration using bio-nanocomposite tissue reinforced with bioactive nanoparticles for femoral defect applications in medicine, Avicenna J. Med. Biotechnol. 12 (2020) 68–76.

[84] S. Esmaeili, H. Akbari Aghdam, M. Motififard, S. Saber-Samandari, A.H. Montazeran, M. Bigonah, E. Sheikhbahaei, A. Khandan, A porous polymeric–hydroxyapatite scaffold used for femur fractures treatment: fabrication, analysis, and simulation, Eur. J. Orthop. Surg. Traumatol. 30 (2020) 123–131, doi:10.1007/s00590-019-02530-3.

[85] M. Monshi, S. Esmaeili, A. Kolooshani, B.K. Moghadas, S. Saber-Samandari, A. Khandan, A novel three-dimensional printing of electroconductive scaffolds for bone cancer therapy application, Nanomed. J. 7 (2020), doi:10.22038/nmj.2020.07.007.

[86] S. Esmaeili, M. Shahali, A. Kordjamshidi, Z. Torkpoor, F. Namdari, S.S. Samandari, M. Ghadiri Nejad, A. Khandan, An artificial blood vessel fabricated by 3D printing for pharmaceutical application, Nanomed. J. 6 (2019), doi:10.22038/nmj.2019.06.00005.

[87] Z. Doozandeh, S. Saber-Samandari, A. Khandan, Preparation of novel arabic gum-C6H9NO biopolymer as a bedsore for wound care application, ACTA (2020), doi:10.18502/acta.v58i10.4915.

[88] A. Raisi, A. Asefnejad, M. Shahali, Z. Kazerouni, A. Kolooshani, S. Saber-Samandari, B. Kamyab Moghadas, A. Khandan, Preparation, characterization, and antibacterial studies of N, O–carboxymethyl chitosan as a wound dressing for bedsore application, Arch.Trauma Res. (2020).

[89] M.A.E.G. El-Sayed Ahmed, L.L. Zhong, C. Shen, Y. Yang, Y. Doi, G.B. Tian, Colistin and its role in the era of antibiotic resistance: an extended review (2000-2019), Emerg. Microbes Infect. 9 (2020) 868–885, doi:10.1080/22221751.2020.1754133.

[90] M.A. Tartanson, L. Soussan, M. Rivallin, S. Pecastaings, C.V. Chis, D. Penaranda, C. Roques, C. Faur, Dynamic mechanisms of the bactericidal action of an Al_2O_3-TiO_2-Ag granular material on an escherichia coli strain, Appl. Environ. Microbiol. 81 (2015) 7135–7142, doi:10.1128/AEM.01950-15.

[91] J.M. Andrews, J.P. Ashby, G.M. Jevons, R. Wise, Tentative minimum inhibitory concentration and zone diameter breakpoints for moxifloxacin using BSAC criteria, J. Antimicrob. Chemother. 44 (1999) 819–822, doi:10.1093/jac/44.6.819.

[92] K.L. Chew, M.V. La, R.T.P. Lin, J.W.P. Teo, Colistin and polymyxin B susceptibility testing for carbapenem-resistant and mcr-positive enterobacteriaceae: comparison of sensititre, microscan, vitek 2, and etest with broth microdilution, J. Clin. Microbiol. 55 (2017) 2609–2616, doi:10.1128/JCM.00268-17.

[93] D. Minardi, M.P. Montanari, E. Tili, I. Cochetti, M. Mingoia, P.E. Varaldo, G. Muzzonigro, Effects of fluoroquinolones on bacterial adhesion and on preformed biofilm of strains isolated from urinary double *J* stents, J. Chemother. 20 (2008) 195–201, doi:10.1179/joc.2008.20.2.195.

[94] M.J. González, L. Robino, V. Iribarnegaray, P. Zunino, P. Scavone, Effect of different antibiotics on biofilm produced by uropathogenic Escherichia coli isolated from children with urinary tract infection, Pathog. Dis. 75 (2017), doi:10.1093/femspd/ftx053.

[95] I. Ozturk, A.N. Yurtman, B. Erac, S. Gul-Yurtsever, S. Ermertcan, M. Hosgor-Limoncu, *In vitro* effect of moxifloxacin and rifampicin on biofilm formation by clinical MRSA isolates, Bratisl. Lek. Listy. 115 (2014) 483–486, doi:10.4149/bll_2014_093.

[96] C. Pérez-Giraldo, C. Gonzalez-Velasco, R.M. Sánchez-Silos, C. Hurtado, M.T. Blanco, A.C. Gómez-García, Moxifloxacin and biofilm production by coagulase-negative staphylococci, Chemotherapy 50 (2004) 101–104, doi:10.1159/000077811.

[97] C. Jacqueline, J. Caillon, Impact of bacterial biofilm on the treatment of prosthetic joint infections, J. Antimicrob. Chemother. 69 (2014) i37–i40, doi:10.1093/jac/dku254.

[98] E.M. Van Wieren, M.D. Seymour, J.W. Peterson, Interaction of the fluoroquinolone antibiotic, ofloxacin, with titanium oxide nanoparticles in water: adsorption and breakdown, Sci. Total Environ. 441 (2012) 1–9, doi:10.1016/j.scitotenv.2012.09.067.

[99] S. Hadiya, X. Liu, W. Abd El-Hammed, M. Elsabahy, S.A. Aly, Levofloxacin-loaded nanoparticles decrease emergence of fluoroquinolone resistance in Escherichia coli, Microb. Drug Resist. 24 (2018) 1098–1107, doi:10.1089/mdr.2017.0304.

[100] H. Gupta, M. Aqil, R.K. Khar, A. Ali, A. Bhatnagar, G. Mittal, Biodegradable levofloxacin nanoparticles for sustained ocular drug delivery, J. Drug Target. 19 (2011) 409–417, doi:10.3109/1061186X.2010.504268.

[101] P. Bagga, H.H. Siddiqui, J. Akhtar, T. Mahmood, M. Zahera, M.S. Khan, Gold nanoparticles conjugated levofloxacin: for improved antibacterial activity over levofloxacin alone, Curr. Drug Deliv. 14 (2017) 1114–1119, doi:10.2174/1567201814666170316113432.

[102] I. Marriott, Apoptosis-associated uncoupling of bone formation and resorption in osteomyelitis, Front Cell Infect. Microbiol. 3 (2013) 101, doi:10.3389/fcimb.2013.00101.

[103] S.K. Sohaebuddin, P.T. Thevenot, D. Baker, J.W. Eaton, L. Tang, Nanomaterial cytotoxicity is composition, size, and cell type dependent, Part Fibre Toxicol. 7 (2010) 22, doi:10.1186/1743-8977-7-22.

[104] S. Lee, J. Kim, K. Ravichandran, H.W. Gil, H. Song, S. Hong, P-glycoprotein induction ameliorates colistin induced nephrotoxicity in cultured human proximal tubular cells, PLoS ONE 10 (2015) e0136075, doi:10.1371/journal.pone.0136075.

[105] B. Sobolewska, J. Hofmann, M.S. Spitzer, K.U. Bartz-Schmidt, P. Szurman, E. Yoeruek, Antiproliferative and cytotoxic properties of moxifloxacin on rat retinal ganglion cells, Curr. Eye Res. 38 (2013) 662–669, doi:10.3109/02713683.2012.746991.

[106] J.J. Aguilera-Correa, A. Garcia-Casas, A. Mediero, D. Romera, F. Mulero, I. Cuevas-López, A. Jiménez-Morales, J. Esteban, A new antibiotic-loaded sol-gel can prevent bacterial prosthetic joint infection: from *in vitro* studies to an *in vivo* model, Front. Microbiol. 10 (2020) 2935, doi:10.3389/fmicb.2019.02935.

[107] A. Ordooei Javan, S. Shokouhi, Z. Sahraei, A review on colistin nephrotoxicity, Eur. J. Clin. Pharmacol. 71 (2015) 801–810, doi:10.1007/s00228-015-1865-4.

[108] J.D. Hartzell, R. Neff, J. Ake, R. Howard, S. Olson, K. Paolino, M. Vishnepolsky, A. Weintrob, G. Wortmann, Nephrotoxicity associated with intravenous colistin (colistimethate sodium) treatment at a tertiary care medical center, Clin. Infect. Dis. 48 (2009) 1724–1728, doi:10.1086/599225.

[109] Z. Gai, S.L. Samodelov, G.A. Kullak-Ublick, M. Visentin, Molecular mechanisms of colistin-induced nephrotoxicity, Molecules 24 (2019), doi:10.3390/molecules24030653.

[110] C. Ho, Y. Chen, F. Hu, C. Yu, P. Yang, K. Luh, Safety of fluoroquinolone use in patients with hepatotoxicity induced by anti-tuberculosis regimens, Clin. Infect. Dis. 48 (2009) 1526–1533, doi:10.1086/598929.

[111] S.M.J. Haeri, Y. Sadeghi, M. Salehi, R.M. Farahani, N. Mohsen, Osteogenic differentiation of human adipose-derived mesenchymal stem cells on gum tragacanth hydrogel, Biologicals 44 (2016) 123–128, doi:10.1016/j.biologicals.2016.03.004.

[112] S. Yona, S. Gordon, From the reticuloendothelial to mononuclear phagocyte system – the unaccounted years, Front. Immunol. 6 (2015), doi:10.3389/fimmu.2015.00328.

[113] J. Baas, N. Senninger, H. Elser, The reticuloendothelial system. An overview of function, pathology and recent methods of measurement, Z. Gastroenterol. 32 (1994) 117–123.

[114] U. Hopf, G. Ramadori, Physiology and pathophysiology of the reticuloendothelial system of the liver (author's transl), Leber Magen Darm 10 (1980) 277–283.
[115] K.L. Streetz, T. Luedde, M.P. Manns, C. Trautwein, Interleukin 6 and liver regeneration, Gut 47 (2000) 309–312, doi:10.1136/gut.47.2.309.
[116] G.R. Wilkinson, Cytochrome P4503A (CYP3A) metabolism: prediction of *in vivo* activity in humans, J. Pharmacokinet. Biopharm. 24 (1996) 475–490, doi:10.1007/BF02353475.
[117] S.B. Yee, The role of Kupffer cells and TNF-alpha in monocrotaline and bacterial lipopolysaccharide-induced liver injury, Toxicol. Sci. 71 (2003) 124–132, doi:10.1093/toxsci/71.1.124.
[118] B. Wang, X. He, Z. Zhang, Y. Zhao, W. Feng, Metabolism of nanomaterials *in vivo* : blood circulation and organ clearance, Acc. Chem. Res. 46 (2013) 761–769, doi:10.1021/ar2003336.
[119] R. Katz, Renal and possibly hepatic toxicity from coly-mycin. Report of a case, Med .Ann. Dist. Columbia 32 (1963) 408–413.
[120] F. Braet, E. Wisse, Structural and functional aspects of liver sinusoidal endothelial cell fenestrae: a review, Comp. Hepatol. 1 (2002) 1, doi:10.1186/1476-5926-1-1.
[121] E. Blanco, H. Shen, M. Ferrari, Principles of nanoparticle design for overcoming biological barriers to drug delivery, Nat. Biotechnol. 33 (2015) 941–951, doi:10.1038/nbt.3330.
[122] B. Ouyang, W. Poon, Y.N. Zhang, Z.P. Lin, B.R. Kingston, A.J. Tavares, Y. Zhang, J. Chen, M.S. Valic, A.M. Syed, P. MacMillan, J. Couture-Senécal, G. Zheng, W.C.W. Chan, The dose threshold for nanoparticle tumour delivery, Nat. Mater. 19 (2020) 1362–1371, doi:10.1038/s41563-020-0755-z.
[123] K. Brandl, V. Kumar, L. Eckmann, Gut-liver axis at the frontier of host-microbial interactions, Am. J. Physiol. Gastrointest. Liver Physiol. 312 (2017) G413–G419, doi:10.1152/ajpgi.00361.2016.
[124] T.A.G. van Vugt, J.M.B. Walraven, J.A.P. Geurts, J.J.C. Arts, Antibiotic-loaded collagen sponges in clinical treatment of chronic osteomyelitis: a systematic review, J. Bone Joint Surg. 100 (2018) 2153–2161, doi:10.2106/JBJS.17.01140.
[125] J.S. Gogia, J.P. Meehan, P.E. Di Cesare, A.A. Jamali, Local antibiotic therapy in osteomyelitis, Semin. Plast. Surg. 23 (2009) 100–107, doi:10.1055/s-0029-1214162.
[126] K.T. Peng, C.F. Chen, I.M. Chu, Y.M. Li, W.H. Hsu, R.W.W. Hsu, P.J. Chang, Treatment of osteomyelitis with teicoplanin-encapsulated biodegradable thermosensitive hydrogel nanoparticles, Biomaterials 31 (2010) 5227–5236, doi:10.1016/j.biomaterials.2010.03.027.
[127] S.W. Jung, S.H. Oh, I.S. Lee, J.H. Byun, J.H. Lee, *In situ* gelling hydrogel with anti-bacterial activity and bone healing property for treatment of osteomyelitis, Tissue Eng. Regen. Med. 16 (2019) 479–490, doi:10.1007/s13770-019-00206-x.
[128] B. Rutledge, D. Huyette, D. Day, J. Anglen, Treatment of osteomyelitis with local antibiotics delivered via bioabsorbable polymer, Clin. Orthop. Relat. Res. 411 (2003) 280–287, doi:10.1097/01.blo.0000065836.93465.ed.
[129] M. Lu, J. Liao, J. Dong, J. Wu, H. Qiu, X. Zhou, J. Li, D. Jiang, T.C. He, Z. Quan, An effective treatment of experimental osteomyelitis using the antimicrobial titanium/silver-containing nHP66 (nano-hydroxyapatite/polyamide-66) nanoscaffold biomaterials, Sci. Rep. 6 (2016) 39174, doi:10.1038/srep39174.
[130] D.M. Zhu, Q.H. Li, Y. Shen, Q. Zhang, Risk factors for quinolone-resistant Escherichia coli infection: a systematic review and meta-analysis, Antimicrob. Resist. Infect. Control 9 (2020) 11, doi:10.1186/s13756-019-0675-3.